AD-A073 382 CALIFORNIA INST OF TECH PASADENA F/G 13/10
LEADING EDGE FLUTTER OF SUPERCAVITATING HYDROFOILS.(U)
MAY 79 C BRENNEN, K OEY, C D BABCOCK N00014-75-C-0379
UNCLASSIFIED ENG-216-1 NL

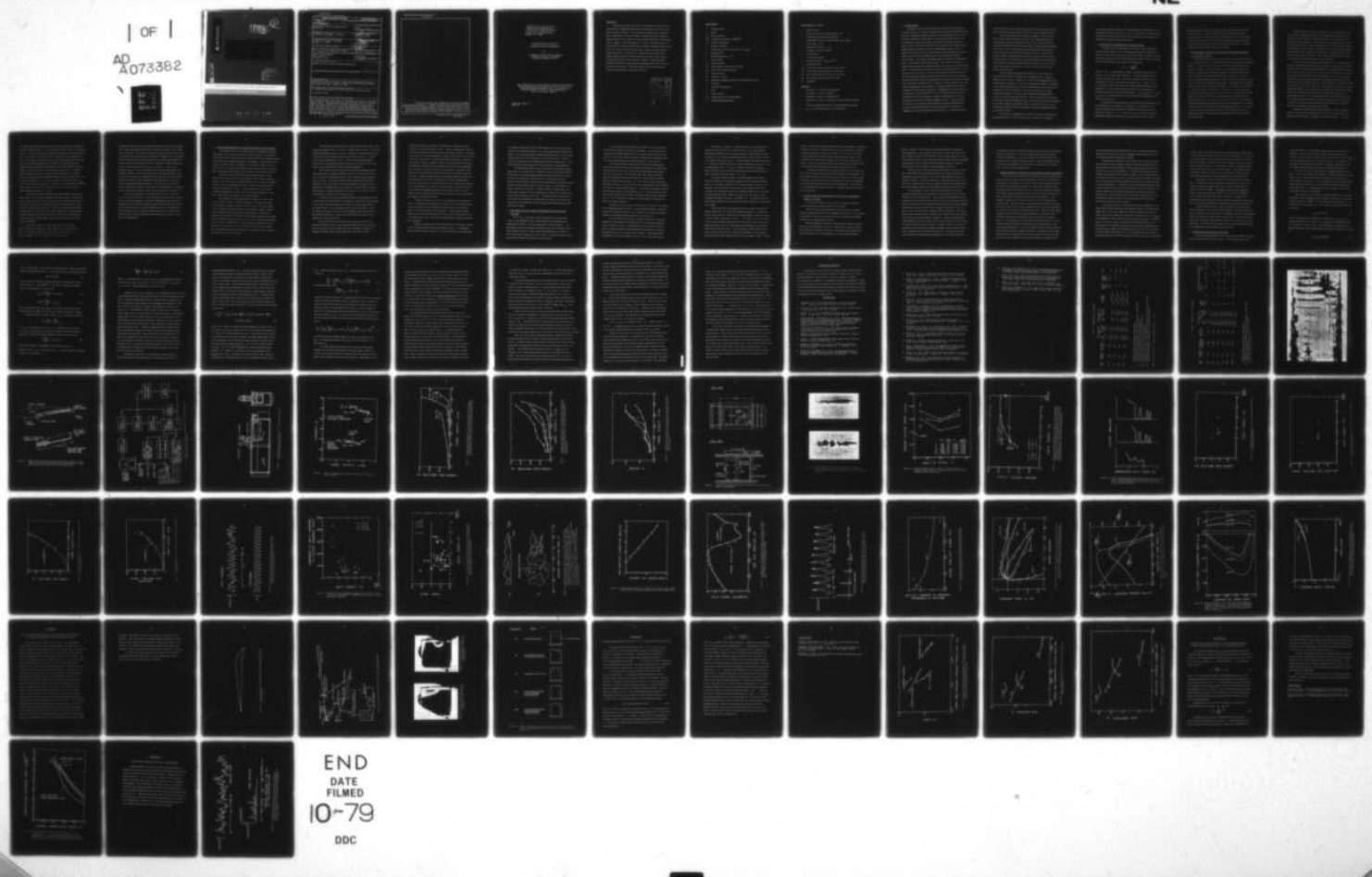

END
DATE FILMED
10-79
DDC

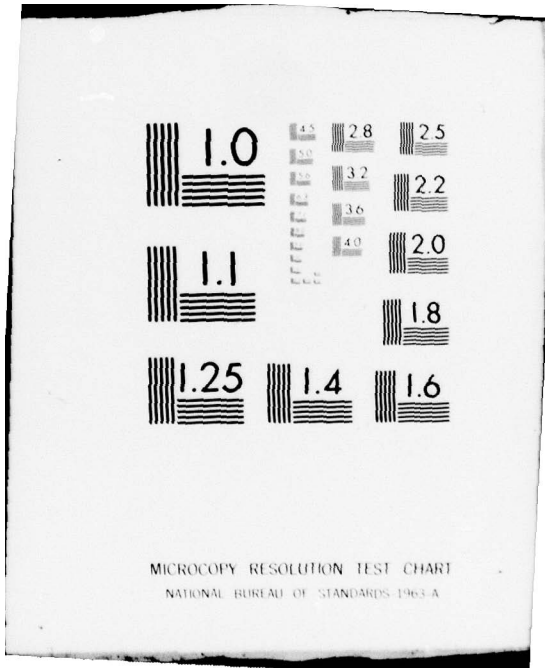
1.0
1.1
1.25
1.4
1.6
1.8
2.0
2.2
2.5
2.8
3.2
3.6
4.0
4.5
5.0
MICROCOPY RESOLUTION TEST CHART
NATIONAL BUREAU OF STANDARDS-1963-A

AD A073382

LEVEL II

DDC FILE COPY.

D D C
RECEIVED
AUG 29 1979
C

CALIFORNIA INSTITUTE OF TECHNOLOGY

PASADENA, CALIFORNIA

79 08 29 043

UNCLASSIFIED

SECURITY CLASSIFICATION OF THIS PAGE (When Data Entered)

REPORT DOCUMENTATION PAGE	READ INSTRUCTIONS BEFORE COMPLETING FORM
1. REPORT NUMBER: Report ENG-216-1 (14)	2. GOVT ACCESSION NO.
3. RECIPIENT'S CATALOG NUMBER	
4. TITLE (and Subtitle): Leading Edge Flutter of Supercavitating Hydrofoils (6)	5. TYPE OF REPORT & PERIOD COVERED: Final rept. (9)
6. PERFORMING ORG. REPORT NUMBER: N/A	
7. AUTHOR(s): C. Brennen, K. Oey and C. D. Babcock (10)	8. CONTRACT OR GRANT NUMBER(s): N00014-75-C-0379 (15) new (16)
9. PERFORMING ORGANIZATION NAME AND ADDRESS: California Institute of Technology, Pasadena, CA 91125	10. PROGRAM ELEMENT, PROJECT, TASK AREA & WORK UNIT NUMBERS: 61153N R02301, SR 023 01 01 (17)
11. CONTROLLING OFFICE NAME AND ADDRESS: David W. Taylor Naval Ship Research and Development Center, (1505), Bethesda, Md 20084	12. REPORT DATE: May 1979 (11)
	13. NUMBER OF PAGES: 78 (12) 83 p.
14. MONITORING AGENCY NAME & ADDRESS (if different from Controlling Office): Office of Naval Research, 800 N. Quincy St, Arlington, Va 22217	15. SECURITY CLASS. (of this report): UNCLASSIFIED
	15a. DECLASSIFICATION/DOWNGRADING SCHEDULE

16. DISTRIBUTION STATEMENT (of this Report)

APPROVED FOR PUBLIC RELEASE; DISTRIBUTION UNLIMITED

DDC RECEIVED AUG 29 1979

17. DISTRIBUTION STATEMENT (of the abstract entered in Block 20, if different from Report)

18. SUPPLEMENTARY NOTES

Sponsored by the Naval Sea Systems Command General Hydromechanics Research Program administered by the David W. Taylor Naval Ship Research and Development Center, Code 1505, Bethesda, Md 20084

19. KEY WORDS (Continue on reverse side if necessary and identify by block number)

(U) supercavitating hydrofoils (U) GHR Program (U) Leading Edge Flutter

(U) Hydrofoil flutter

79 08 29 043

20. ABSTRACT (Continue on reverse side if necessary and identify by block number)

This document represents the results of experiments and analysis of the phenomenon of leading edge flutter which has been observed to occur for supercavitating hydrofoils. The experiments confirmed the existence of such a single degree of freedom flutter involving chordwise bending and indicated that for long, natural (or vapor-filled) cavities the reduced flutter speed, $U_F/\omega_F c$ was in the range 0.15 to 0.23. Secondary effects observed were the variation with the angle of attached (a minimum flutter speed occurred at 10^0) and with

DD FORM 1 JAN 73 1473 EDITION OF 1 NOV 65 IS OBSOLETE
S/N 0102-LF-014-6601

071 550

U sub F / omega sub F c 10 deg

SECURITY CLASSIFICATION OF THIS PAGE (When Data Entered)

CONT

a foil mass ratio. Shorter cavities typically yielded flower flutter speeds due to a complex interaction between the bubble collapse process occurring in the cavity closure region and the unsteady hydrodynamic load on the foil. Finally a relatively simple theoretical analysis for supercavitating hydrofoils with elastic axes aft of mid-chord is presented. This linear analysis yields reduced flutter velocities somewhat lower than those observed.

SPONSORED BY THE NAVAL SEA SYSTEMS COMMAND GENERAL HYDROMECHANICS RESEARCH (GHR) PROGRAM ADMINISTERED BY THE DAVID W. TAYLOR NAVAL SHIP RESEARCH AND DEVELOPMENT CENTER, BETHESDA, MD 20084

LEADING EDGE FLUTTER OF SUPERCAVITATING HYDROFOILS

by

C. Brennen, K. Oey, and C.D. Babcock
California Institute of Technology
Pasadena, California 91125

This research was carried out with the support from the General Hydrodynamics Research Program of the David Taylor Naval Ship Research and Development Center, Carderock, Md. (Contract N00014-75-C-0379). This constitutes the final report on that program.

Report No. Eng. 216.1
May 1979

ABSTRACT

This paper presents the results of experiments and analysis of the phenomenon of leading edge flutter which has been observed to occur for supercavitating hydrofoils. The experiments confirmed the existence of such a single degree of freedom flutter involving chordwise bending and indicated that for long, natural (or vapor-filled) cavities the reduced flutter speed, $U_F/\omega_F c$, was in the range 0.15 to 0.23. Secondary effects observed were the variation with the angle of attack (a minimum flutter speed occurred at 10^o) and with a foil mass ratio. Shorter cavities typically yielded lower flutter speeds due to a complex interaction between the bubble collapse process occurring in the cavity closure region and the unsteady hydrodynamic load on the foil. Finally a relatively simple theoretical analysis for supercavitating hydrofoils with elastic axes aft of mid-chord is presented. This linear analysis yields reduced flutter velocities somewhat lower than those observed.

Accession For
NTIS GRA&I
DDC TAB
Unannounced
Justification
By
Distribution/
Availability Codes
Dist | Available/or special
A

Nomenclature

a	Flexible chord
c	Chord
C_D	Drag coefficient
C_M	Coefficient of moment, $M/\frac{1}{2}\rho U^2 c^2$
E	Modulus of elasticity
I	Moment of inertia
I_o	Dimensionless moment of inertia, $I = I_o \rho_s t c^2$
j	Imaginary unit
k	Reduced frequency, $\omega c/U$
ℓ	Cavity length
K	Spring constant
M	Hydrodynamic moment per unit span
p_∞	Free stream tunnel pressure
p_c	Cavity pressure
Q	Q-factor, $\omega_N/\Delta\omega$
R	Equivalent cylindrical radius of the pinched-off cavity
s	Foil span
t	Flexible foil thickness
T	Time
U	Tunnel velocity
U_D	Tunnel velocity for foil divergence
y	Leading edge displacement

Nomenclature (continued)

α	Angle of attack
β	Distance of hinge from leading edge is βc
δ	Leading edge displacement amplitude
λ	Wavelength of waves on leading edge cavity surface
μ	Mass ratio, $\rho_s t/\rho c$
μ^*	Modified mass ratio, $\rho_s t/\rho a$
ν	Kinematic viscosity of liquid
ρ	Liquid density
ρ_s	Foil material density
σ	Cavitation number, $(p_\infty - p_c)/\frac{1}{2}\rho U^2$
ω	Radian frequency
ω_{NV}	First mode natural frequency of foil in vacuo
ω_A	First mode natural frequency of foil in air
ω_W	First mode natural frequency in "still" water
ω_N	First mode natural frequency with flow
$\Delta\omega$	Bandwidth

Modifiers

Subscript 0 refers to mean quantities

Subscript R refers to real part

Subscript I refers to imaginary part

Subscript F refers to quantities at critical flutter conditions

Tilda over character refers to complex fluctuating quantity.

Dot over character denotes time derivative.

1. INTRODUCTION

Hydrofoils utilized for hydrofoil boats, propeller blades and pump or turbine blades are, of course, subject to the same kinds of fluid/structure interaction instabilities which had earlier been investigated in the context of airfoils (Abramson, (1969)). However increasing speeds led to the need to redesign foil shapes so that they could operate efficiently with large attached vapor or gas filled cavities; such redesigns involve relatively thin wedge-shaped foils with sharp and thin leading edges (Acosta, 1973). It has become apparent that such foils operating with fully-developed cavities exhibit a hydro-elastic instability which has no equivalent in subsonic aero-elasticity. This flutter phenomenon which we shall call "leading edge flutter" is the subject of the present report. One of the earliest and unexpected observations of leading edge flutter was made by Waid and Lindberg (1957). During performance tests of certain supercavitating foils in a water tunnel, they observed that at a certain critical speed the forward portion of the foil including the leading edge began to vibrate violently in a chordwise bending mode while the thick trailing edge part of the foil remained stationary. One result of this vibration was the creation of a train of waves on the cavity surface originating at the leading edge (a photograph taken from Waid and Lindberg (1957) is included as figure 1). Subsequently it has been observed by Spangler (1966); also Rothblum, Mayer and Wilburn (1969) have noted radical and deleterious changes in the hydro-elastic behavior of surface-piercing struts when these develop ventilated cavities. The phenomenon has also been observed with supercavitating propellers (English (1978)) and some leading edge failures in supercavitating inducer pumps are suggestive of a similar phenomenon (Gross (1975)). In practical situations

one must be concerned with unbounded flutter motions; even if non-linear effects limit the flutter amplitude there is the threat of fatigue failure.

These sketchy and early observations suggest (correctly as will be seen) that leading edge flutter requires only a single elastic mode, namely that of chordwise bending of the foil. This contrasts with conventional wing flutter which involves two modes (usually spanwise bending and torsion; or more fundamentally pitching and heaving) interacting in such a way that the foil absorbs energy from the flow. Woods (1957), Kaplan and Henry (1960) and Song (1972) have examined the conventional flutter potential for cavitating (or separated) flow theoretically and Song and Almo (1967), Kaplan and Lehman (1966) and others have performed conventional flutter experiments. Further discussion on these will be delayed until Section 8.

One other phenomenon demands mention: it is well-known that hydrofoils with cavities extending from the leading edge to a length of between about $\frac{1}{2}$ and $1\frac{1}{2}$ chords (i.e. closure in the neighborhood of the trailing edge) are unstable at almost any speed; the lift exhibits oscillations as the cavity oscillates between closure on the suction surface and a point downstream of the trailing edge. This will be referred to as partial cavitation instability; it is a purely fluid mechanical instability which would occur with a completely rigid foil. However when the foil is flexible the partial cavitation instability can lock into the natural structural frequency. In the context of the present study it will be seen that there is an overlap between leading edge flutter and partial cavitation instability when the cavity length is short.

The present investigation was designed to concentrate primarily on leading edge flutter for long, fully-developed cavities and to minimize

the complexities which might occur with the appearance of hybrid forms of instability such as discussed above. The experimental observations will be described first: they will be followed by some theoretical considerations which help to explain the basic phenomenon.

2. PRELIMINARY EXPERIMENTAL CONSIDERATIONS

Consider first the dimensionless parameters which might govern the hydro-elastic behavior of a cavitating hydrofoil which is rigidly fixed near the trailing edge but capable of chordwise bending. The lowest natural structural frequency of chordwise bending in the absence of any surrounding fluid will be denoted by ω_{NV} and this will be given by

$$\omega_{NV} = C_1 \frac{t}{c^2} \sqrt{\frac{E}{\rho_s}} \tag{1}$$

where E and ρ_s are the elastic modulus and density of the material of the foil, t is a representative thickness, c the chord length and C_1 some constant of order unity. The inertial effects of a static fluid surrounding the flow are represented by the mass ratio $\mu = \rho_s t/\rho c$ where ρ is the fluid density. The velocity and angle of attack of the flow will be denoted by U and α while the extent and effect of cavitation will, as usual be represented by the cavitation number $\sigma = (p_\infty - p_c) \Big/ \frac{1}{2} \rho U^2$, where p_∞ and p_c are respectively a reference pressure far upstream and the pressure in the cavity.

If the fluid is assumed inviscid, incompressible and unbounded and the cavitating foil is oscillated at a frequency ω the complete list of pertinent dimensionless parameters in addition to geometric foil shape factors is: ω/ω_{NV}, k, σ, μ, α where $k = \omega c/U$ is the reduced frequency. The experiments were intended to seek out the nature of the relations

between these quantities for leading edge flutter whose frequency will be denoted by $\omega = \omega_F$. Other parameters such as the Reynolds number, Weber number, Froude number and thermodynamic factors could be added to the above list but were not separately investigated in the present study. Perhaps the most important of these is the Reynolds number, Uc/ν, which ranged from 10^6 to 3×10^6 in the tests conducted.

3. EXCITATION SYSTEMS AND THE VIBRATION CHARACTERISTICS OF THE MODEL FOILS.

The foils tested were intended to model the gross structural features of supercavitating foils yet be simple enough to be manufactured in significant number. As shown in figure 2 they consisted of thin flat aluminum plates (6061 T-6 aluminum) of various thickness; at the trailing edge they were bolted to a much thicker and stiffer mounting bar which essentially fixed the rear portion and trailing edge of the foils. All foils had a chord of 15.24 cm and their leading edges were machined with a 30° wedge to produce a clean, sharp cavity separation at this point. The length of the cantilevered flexible portion of the foil will be denoted by a ; consequently the parameter a/c should be added to the list in the last section in order to represent the specific foil geometry used. Experiments were carried out in two water tunnels, the FSWT and HSWT (see below); the span of the foils tested in these facilities were respectively 35.56 cm. and 15.24 cm. The foils were each fitted with three strain gauges bonded to the suction side of the flexible portion in order to monitor chordwise bending; the three gages were placed at mid-span and near the ends of the span. One additional gage on the mounting bar registered the fluctuating lift (actually the force normal to the mounting bar).

Most hydrofoils, propellers or pump blades are supported in such a way that their modes of vibration are quite complicated; nodal lines do not lie simply in the chordwise or spanwise direction. As an illustration of this we include in Appendix A the results of an investigation into the natural frequencies and modes of a supercavitating hydrofoil model which was tested in the High Speed Water Tunnel at Caltech as part of an earlier investigation (Ward (1976)). Other examples of mode shapes are contained in the studies of Osterwalder and Sonsino (1975). However the present foils were deliberately intended to have fairly simple modes of vibration.

The first natural frequencies of the model foils in air were measured by tuned excitation using an acoustical loudspeaker. These values are listed in Tables 1 and 2 along with the foil thicknesses, foil designations and other data; Tables 1 and 2 are for the 35.56 and 15.24 cm. span foils respectively. The first mode involved pure chordwise bending in every case; the second mode was similar except that the phase of the bending varied over the span with the ends out of phase by 180° and a node at mid-span. (With the 35.56 cm. span foils the third and fourth modes respectively involved spanwise phase change with nodes at two locations and the second mode of chordwise bending with a node at about mid-chord and little spanwise phase change). The experimental values in air are compared in Tables 1 and 2 with theoretical values obtained using the method described by Barton (1951) for vibration in a vaccuum. The agreement is fairly good and the difference is probably due to the aerodynamic damping and added mass.

A different excitation system was developed for tests under water. This was used for bench testing in tanks of "still" water and in one of the water tunnel experiments; a schematic is included as figure 3. A music

wire attached to the leading edge (usually near mid-span) was connected to an electromagnetic shaker. A weak spring and a load cell were interposed in the wire. The spring allowed decoupling of the motion of the shaker and the foil. The purpose of the load cell was to monitor the force applied to the foil. Since frequency response spectra are most meaningful when the peak to peak. value of the applied force is constant, a feedback system was installed which automatically adjusted the motion of the shaker to ensure a constant preset level of force as monitored by the load cell. Using this system frequency response spectra of the foil displacement as monitor by the foil strain gauges were obtained using relatively low sweep rates. The half-power bandwidth, $\Delta\omega$, about the resonant or natural frequency ω_N indicated the amount of damping for a particular foil under the given conditions of flow (angle of attack, etc.); this data will be presented as Q-factors defined in the usual way as $Q = \omega_N/\Delta\omega$.

This procedure worked well except in the following circumstances. When used at or near flutter conditions in the water tunnel, a certain level of force appeared across the load cell due to compression or extension of the spring. As long as this component of force was less than the chosen level of excitation force all was well. But if it exceeded the chosen level the shaker was incapable of the necessary compensation which would have required removing power from the system. Under these conditions the spectra were less valuable and the resulting Q-factors could not be considered meaningful.

In the bench tests in air this excitation system yielded natural frequencies identical to those obtained by acoustical excitation. The natural frequencies, measured in "still" water are listed in Tables 1 and 2. They are compared in that

table with the theoretical values obtained using the strip theory of Lindholm, Kana, Chu and Abramson (1965) which incorporates estimates of the added mass of the water. The large discrepancies between theory and experiment are similar to the discrepancies recognized by Lindholm et al in comparison with their experiments; there would appear to be considerable difficulties involved in the accurate prediction of the "still water" natural frequencies for foils with span/chord ratios of one or greater. Some of the difficulty may be due to lack of validity of the strip theory though viscous and eddy shedding characteristics of the real flow may also play a role. The theoretical values are substantially lower than the observations indicating that the amount of fluid contributing to the added mass is much less than that anticipated by the strip theory. Later it will be seen that the natural frequencies (and flutter frequencies) of foil vibration in a cavitating flow are quite close to those in "still" water (see section 4 and figure 5).

Some measurements of the damping of the 35.56 cm. span foils were also made in "still water". The principal conclusion of this investigation as reported in Appendix B was that the damping was non-linear and dependent on the oscillatory Reynolds number associated with the vibration. These measurements are only of incidental interest since the damping is quite dependent on viscous and eddy shedding effects at the leading edge and these effects would probably be significantly different in the presence of an oncoming stream.

4. INITIAL EXPERIMENTS IN THE FREE SURFACE WATER TUNNEL.

In the absence of any prior experimental investigations of leading edge flutter it was deemed necessary to conduct a series of preliminary experiments in the Free Surface Water Tunnel (FSWT) in the Hydrodynamics Laboratory at the California Institute of Technology. This tunnel operates with a free surface open to atmosphere at speeds up to about 7.6 m/sec. The 35.56 cm. span foils were rigidly mounted in the tunnel as depicted in figure 4; both the depth of immersion and angle of attack could be varied.

Since the velocity of this tunnel was not high enough to create natural vapor-filled cavities, air was supplied to the suction surface by means of an array of forward pointing tubes in order to generate ventilated cavities. This arrangement allowed the creation of ventilated cavities above tunnel speeds of 1.2 m/sec.; above about 5m/sec. the cavities ventilated to atmosphere via the surface piercing supporting struts and hence the artificial air supply was no longer necessary.

When ventilated to the atmosphere the cavities were quite long (>1 m.) and were similar to choked conditions in a closed water tunnel. With artificial ventilation at speeds less than 5 m/sec. the cavity length could be adjusted to a limited extent by varying the air supply. However it was determined that this had only a minor influence on the flutter characteristics and since the effect of cavity length is much better defined in the later HSWT tests (see Sections 5, 6) we shall confine the presentation here to results for long cavities. Typical artificial ventilation rates required were of the order of 2.5×10^{-4} standard m^3/sec.; larger values were avoided because the air jets within the cavity then caused significant distortion of the cavity free surface.

The two thinnest foils (F16 and F31, table 1) yielded little information; the first diverged at 1.2 m/sec. before a cavity could be created. The second exhibited unbounded flutter as soon as a ventilated cavity was formed at the lowest speed at which this was possible (also about 1.2 m/sec.). Without a cavity it diverged about 2.1 m/sec. These non-cavitating divergence speeds are in fair agreement with theoretical values listed in Table 1 and derived by the approximate method outlined in Appendix C.

The two thicker foils (F61 and F89, Table 1) both exhibited leading edge flutter under cavitating conditions. On the other hand in the absence of a cavity they remained quiescent up to the maximum tunnel velocity of about 7.6 m/sec. This agrees with the observation that the theoretical divergence speeds for both non-separated potential flow and for cavity or wake flow are all higher than this (see Table 1). Hence the tests confirmed the dominance of leading-edge flutter in the hydro-elastic behavior of the cavitating foils cantilevered at the trailing edge.

Frequency response investigations using the electromagnetic shaker mounted above the tunnel (Section 3 and figure 4) showed that in the presence of a cavity the natural frequency of the foils was virtually independent of the angle of attack, cavity ventilation rate or level of excitation. Indeed as confirmed by figure 5 it decreased only slightly with tunnel velocity so that ultimately the flutter frequency was little different from the natural frequency at subcritical speeds.

The onset of flutter as the speed was increased was much less dramatic in these tests than in the subsequent HSWT tests; the reason for this is not entirely clear but may be due to the additional compliance or damping associated with air-filled rather than vapor-filled cavities.

Typical leading-edge displacement magnitudes as a function of tunnel velocity are presented in figures 6 and 7. Figure 6 typifies the results in the absence of shaker excitation and at various angles of attack. The flutter speed appears to depend somewhat on the angle of attack but is of the order of 4 m/sec. and 7 m/sec. for foils F61 and F89 respectively. However it was possible to operate at higher speeds as illustrated by the F61 results. The amplitude of the limit cycle oscillation merely increased suggesting the presence of strongly non-linear viscous damping. The effect of the angle of attack was typical of that discerned in all of the tests reported in this paper. It appeared that the flutter speed had a slight minimum in the neighborhood of about $\alpha \approx 10^{o}$ with flutter occurring at slightly higher values for either larger or smaller angles of attack. Steady state performance measurements were made to determine whether the steady state lift slope exhibited any significant change at this angle of attack. No such change could be discerned; indeed the lift slope appeared to remain constant up to angles of attack of about 20^{o}.

Frequency response spectra were also obtained with a number of different amplitudes of excitation force (0.111, 0.222, and 0.444 Newtons). Typical peak displacement amplitudes and Q-factors are presented in figures 7 and 8 as functions of tunnel velocity. The external excitation appeared to cause the displacement to increase more gradually than it did in the flutter onset tests. The Q-factor graph similarly suggests a gradual loss of damping.

Finally, questions arose concerning the effect of the shape or finish of the foil leading edge on the observed onset of flutter. To investigate this two different shapes of plastic cover were fitted over the leading edge.

No significant differences in the flutter behavior were observed when the foils were run with these plastic covers. The separation point without the plastic covers remained fixed at the knife edge though there was occasional wetting of part of the 30° finishing face on the suction surface. With the covers the separation point oscillated back and forth during flutter. This did not apparently effect the gross dynamic features of the phenomenon.

In summary the FSWT tests (i) confirmed the existence of leading edge flutter for cavitating foils, and that it occurred at speeds well below the divergence speed (ii) suggested that such flutter did not occur in the absence of a cavity; then the foils may well remain quiescent all the way up to the divergence speed (iii) that though the angle of attack had some effect the reduced flutter speed ($U_F/\omega_F C$ where ω_F is the flutter frequency) seemed to be about 0.11 (iv) that the flutter frequency was close to the natural frequency of the cavitating foil in subcritical conditions and to the natural frequency in still water. The HSWT tests described in the next section were undertaken to extend the observations to a wider range of speeds and foil stiffnesses and to investigate the phenomena for natural vapor-filled cavities.

5. HIGH SPEED WATER TUNNEL EXPERIMENTS WITH NATURAL CAVITIES.

The 15.24 cm. span foils were tested with natural vapor-filled cavities in the High Speed Water Tunnel (HSWT) of the Hydrodynamics Laboratory at Caltech. The mounting system is shown in figure 9. The independent velocity and pressure regulation in this tunnel allowed observations of flutter onset for a wider range of foil thicknesses (see Table 2) over a wide range of speeds (4.5 to 18.5 m/sec.), angles of attack (7 to 13°) and cavitation numbers (from short to long cavities).

In contrast to the observations in the FSWT, the onset of flutter in the HSWT was sudden, dramatic and repeatable. It could not only be recognized by the sudden appearance of a sinusoidal output from the strain gauges but was also visible and audible. Furthermore the appearance of the cavity would change as illustrated by figure 10 (see Section 7).

The flutter speed for a given foil at a particular angle of attack was lower for shorter cavities but tended to asymptote to a certain value for long cavities (see below). These long cavity flutter speeds ranged from 8.5 to 19.8 m/sec. for foils H68, H89, H125, H50 A and H125 B (foil H31 diverged and was destroyed before a cavity could be formed). However when the flutter speeds, U_F, were non-dimensionalized using the flutter frequency, ω_F (see Table 2), the resulting values all lay between 0.15 and 0.23 as illustrated in figure 11. The arrows in this figure indicate that the flutter speeds for H68 and H50 A at $\alpha = 7^o$ had not reached a clear limit for the longest cavity conditions examined; also the flutter speed for H125 at $\alpha = 13^o$ seemed to be a little above the maximum velocity of the tunnel under these conditions.

It follows that $U_F \approx 0.15\, \omega_F c$ could be used as a first order estimate of the leading edge flutter speed of a supercavitating hydrofoil. All that is required is the flutter frequency, ω_F, which is close to the first natural frequency of chordwise bending under water (see Section 3).

As in the FSWT tests, an angle of attack of about 10^o consistently manifest the lowest flutter speed (see figure 11); as previously stated the reason for this is not clear. It should also be recorded that a few spot checks at negative angles of attack indicated identical flutter speeds and flow patterns to those at a positive angle of attack. This eliminated the possibility of any Froude number or buoyancy effect in the phenomenon.

The values of $U_F/\omega_F c$ for different foils seem to be shifted up or down by the same amount at all angles of attack. If we assume that the individual foil stiffnesses are already accounted for by the different flutter frequencies, ω_F, then the remaining parameters which could account for these shifts are the mass ratio, μ, and the flexible chord/total chord ratio, a/c. Collation of the data in figure 11 with the tabulated values of a/c and a modified mass ratio, $\mu^* = \rho_s t/\rho a$ included in that figure suggests a fairly consistent increase in the reduced flutter speed with increasing μ^* and no consistent trend with either a/c or ω_F.

The effect of cavity length (or cavitation number) on the flutter speed was similar for all foils and is typified by the results presented in figure 12. For angles of attack of 10° and above there was only a very slight decrease in the flutter speed as the cavity length was decreased. At lengths less than about 2 chords the amplitude would increase markedly as the leading edge flutter phenomenon began to merge with the partial cavitation instability (see Section 1 and figure 12). The danger of foil and tunnel damage limited the experiments that could be performed in this short cavity regime.

Cavity length had a more marked effect on the flutter speed at the smaller angles of attack (7° and 8°) as indicated in figure 12. In addition to the decrease in flutter speed with decreasing length, a rather interesting "resonant length" phenomena occurred. The experiments were often carried out by setting the tunnel speed at a value just a little less than the long cavity flutter speed and subsequently decreasing the cavity length by increasing the tunnel pressure. At the low angles of attack flutter would occur at some cavity length but subsequently disappear as the length was decreased only to appear again at another resonant length. These "resonant

lengths" were generally integer multiples of the chord length as illustrated by figure 13 which is a qualitative sketch of the variation in the amplitude of leading edge displacement (for foil H89 at $\alpha = 7^{o}$) for three different speeds progressively further from the long cavity flutter speed. This accounts for the hatched area in figure 12 where all the onset points are plotted. This effect undoubtedly represents the influence on flutter of the cavity pinch-off and collapse phenomenon described in Section 7.

Finally it is important to record that the foils were also tested in wake flow at tunnel pressures high enough to suppress all cavitation. No sign of flutter could be detected in any of these tests even when the tunnel velocity was much larger than the cavitating flutter speed (see Appendix D for incidental data on the wake pressure fluctuations). It seemed that no other phenomena would occur before reaching the divergence speed for these wake flows.

6. OSCILLATING LOAD, DISPLACEMENT AND CAVITY PRESSURE DURING FLUTTER.

The purpose of this section is to record a number of detailed measurements made during the flutter tests in HSWT.

Both the leading edge displacement (from the foil strain gages) and the oscillating load (from the mounting bar strain gage) were recorded during flutter and spectral analysis and cross correlation subsequently performed on a digital signal processor.

Both the displacement and the oscillating load varied with angle of attack and cavity length for a given foil. At the larger angles of attack (10^{o} and greater) the flutter speed was constant with cavity length; hence typical displacement and load amplitudes are plotted against length in

figures 14 and 15. These indicate increasing amplitudes of flutter with decreasing length, a fact referred to previously. On the other hand at the lower angles of attack (7^{o}, 8^{o}) the flutter speed changes significantly with cavity length. In this case the variation with speed rather than cavity length is most apparent and not unexpectedly both amplitudes appear to increase with the square of the velocity as typified by figures 16 and 17.

Both signals were quite sinusoidal during flutter and cross-correlation confirmed that the load (positive upward) was in phase with the foil displacement (positive upward). This seems superficially at odds with a resonant condition. However it should be recognized that the foil alone in the absence of any water or flow has a natural frequency much higher than the flutter frequency; hence one would expect this in-phase characteristic.

Measurements were also made of the oscillations in the cavity pressure during flutter; a piezoelectric pressure transducer was mounted within the cavity for this purpose. These measurements indicated that the magnitude of the oscillating cavity pressure was very small (about $400 N/m^2$) and its contribution to the oscillating load on the foil was virtually negligible. Though the traces were rather noisy (see figure 18) the basic flutter frequency could be discerned in the signal from the transducer. The magnitudes at the fundamental flutter frequency were obtained by spectral analysis and all values are plotted together in figure 19. They are plotted against cavity length because there appear to be a rough trend for larger oscillating cavity pressures with shorter cavities. No other trends were evident; for example the cavity pressure oscillations did <u>not</u> increase with foil displacement, indeed the reverse seemed to be the case. The phase between the cavity pressure oscillation and the displacement is presented in figure 20

and suggests no great consistency though the cavity pressure generally lags behind the displacement. All of this suggests that the cavity pressure oscillations play little or no role in the dynamics of flutter and that the cavity pressure remains essentially constant. This is consistent with the fact that the thermodynamic time constant for vaporization is extremely short in water at normal temperatures.

7. OBSERVATIONS OF THE FLOW IN THE REGION OF CAVITY CLOSURE.

This section will be devoted to a description of the interesting events which occurred at cavity closure during flutter. Earlier we remarked on the change in the appearance of cavity closure and cavity wake when flutter occurred; this is illustrated in figure 10. Upon closer inspection using high speed movies taken at 600 frames/sec. the following picture emerged. The leading edge movement during flutter produces a train of waves on the upper cavity surface as sketched in the upper part of figure 21. The amplitude of these waves increases as they are convected downstream (see figure 22). As seen from the cavity interior the crests become quite sharp and a portion of the cavity is pinched off when these crests approach the cavity closure region as indicated in figure 21. There are some smaller amplitude waves on the lower surface which play a much lesser role. A detailed frame by frame tracing of the pinch-off process is included in figure 21. The resulting "separated bubble" had the appearance of a cloud of small bubbles; the interior may however have contained larger voids. It also had the appearance of a pair of cavitated vortices with the upper and lower surfaces rotating in opposite directions. Consequently the periodic pinching off also constituted the elements of a Karman vortex street with pairs of vortices imbedded in each separated bubble; clearly this feature

is associated with the oscillating lift on the foil. It should be noted that Karman vortex streets in the wake of steady cavitating flows have been observed previously (Young and Holl (1966)).

The situation was further complicated by the fact that shortly after pinch-off these clouds of bubbles collapsed; subsequent rebounds and collapses followed in synchronization with the flutter frequency as the whole structure was convected downstream. A typical volume history for this collapse and rebound process is shown in figure 23 for foil H89 fluttering at a tunnel speed of about 7.9 m/sec. with a frequency of 60 Hz; the radius of the volumetrically equivalent cylinder for a particular separated bubble is plotted against time. (It should be noted that the significant three-dimensionality could be discerned in the structure after the first rebound.) One should visualize a train of these structures each separated in time by a flutter period. The time between pinch-off and first collapse varied considerably with different foils and flow configurations and ranged from almost zero up to about 2 flutter periods.

The question arose as to whether the pressure perturbations in the liquid which would be generated by the periodic collapse of the pinched-off bubble clouds could cause sufficient oscillatory loading on the pressure surface of the foil to generate a closed-loop resonant system. One estimate of the magnitude of this radiated pressure perturbation would be $2\rho R(\dot{R})^2/r$ where R, $\dot{R}$ are the radius of the bubble and its time derivative and r is the distance to the sensing point (this is based somewhat unrealistically on spherical bubble collapse). Taking typical values of R and $\dot{R}$ from figure 23 and the length of the cavity for r such calculations result in values of the oscillating pressure at the foil which are of the same order of magnitude

as those required to cause the observed oscillating lift (about 3000 N/m^2). To examine this further a piezo-electric pressure transducer was mounted in the tunnel wall to monitor the fluctuating pressure in the water close to the closure region. A typical trace and power spectrum for such measurements is shown in figure 24. The harmonic content is consistent with the violent and non-linear process of cavity collapse. The magnitude of the fundamental component did indeed decay with distance from the closure region indicated in figure 25 and its magnitude was about 3000 N/m^2.

All of this is consistent with the closed loop resonance mentioned above. Furthermore cross-correlations revealed that the pressure perturbations and the foil displacement could either be in-phase with one another or 180^o out of phase. Any lightly damped system would yield similar results. Since the phase shift is very abrupt one is unlikely to detect the theoretical 90^o phase shift at resonance. Furthermore it could explain why the flutter speed decreased with decreasing cavity length since the pressure perturbations encountered by the foil are then greater.

Despite all this, the above does not constitute proof that the postulated mechanism is the primary reason for flutter It will be shown in the next section that leading edge flutter for cavitating hydrofoils can be explained without any reference to these closure region events. Nevertheless there seems little doubt that the phenomena is in some way affected by the closure phenomena. The effect of cavity length and the resonant length phenomena are probably outward manifestations of this influence.

8. THEORETICAL ANALYSES OF FLUTTER.

The experimental program indicates that leading edge flutter depends not only on the reduced velocity $U_F/\omega_F c$ but also to some extent on the

cavitation number (or cavity length), angle of attack and the mass ratio parameter. In this section we shall explore a simple model for this phenomenon and attempt to collate the observations with previous investigations of conventional flutter for cavitating hydrofoils. It can however be anticipated that no single model of such a complicated unsteady flow will be capable of explaining all the observed experimental observations.

Perhaps the simplest model is that of a rigid foil hinged at some point at or near the trailing edge; the effective spring constant of the spring which restrains rotational motion about this hinge will be denoted by K. This hypothetical foil (chord, c) can be thought of as performing oscillatory motion identical to that of the zero lift line of the actual foil undergoing leading edge flutter. The hinge position will be denoted by β where βc is its distance from the leading edge.

Such a model is of course similar to that employed for conventional wing flutter analyses except that the possibility of additional heave motion of the hinge point is excluded. The instantaneous angle of attack, α, is subdivided into a mean angle, α_o, and a small time dependent component, according to

$$\alpha = \alpha_o + \mathrm{Re}\left\{\tilde{\alpha}\, e^{j\omega T}\right\} \tag{2}$$

where $\tilde{\alpha}$ represents the magnitude of the oscillations, $\omega = \omega_R + j\omega_I$ is a complex frequency and T is time. It is convenient to establish the origin of T such that $\tilde{\alpha}$ is purely real. The hydrodynamic moment about the hinge point (positive in the leading edge up direction) is similarly represented as

$$M = M_o + \mathrm{Re}\left\{\tilde{M}\, e^{j\omega T}\right\} \tag{3}$$

where $\tilde{M} = \tilde{M}_R + j\tilde{M}_I$ is necessarily complex in general. Then if the effective moment of inertia of the foil is I, the equation of the perturbations becomes

$$\tilde{\alpha}(K - \omega^2 I) = \tilde{M} \tag{4}$$

If the coefficient of moment about the hinge point is defined in the conventional manner as, $C_M = M/\frac{1}{2}\rho U^2 c^2$, and $\tilde{M}/\tilde{\alpha}$ is replaced by $d\tilde{M}/d\tilde{\alpha}$ the real and imaginary parts of (4) yield

$$\tfrac{1}{2}\rho U^2 c^2 \frac{d\tilde{C}_{MR}}{d\tilde{\alpha}} = K - I(\omega_R^2 - \omega_I^2) \tag{5}$$

$$\tfrac{1}{2}\rho U^2 c^2 \frac{d\tilde{C}_{MI}}{d\tilde{\alpha}} = -2I\omega_R\omega_I \tag{6}$$

where the quantity $\tilde{C}_M = \tilde{C}_{MR} + j\tilde{C}_{MI}$ will be obtained from the unsteady hydrodynamics and will be a function of the reduced frequency, $k = \omega_R c/U$.

It follows that the divergence speed, U_D, (if it exists) is given by

$$U_D^2 = 2K \Big/ \rho c^2 \left(\frac{d\tilde{C}_M}{d\tilde{\alpha}}\right)_{k=0} \tag{7}$$

On the other hand flutter may occur if ω_I is negative for any non-zero value of ω_R; this implies from equation (6) that the system is unstable if $dC_{MI}/d\tilde{\alpha} > 0$ and that the neutral stability or flutter point is given by

$$\left(\frac{d\tilde{C}_{MI}}{d\tilde{\alpha}}\right) = 0 \quad \text{for} \quad \omega_R \neq 0 \quad . \tag{8}$$

This will determine a reduced flutter frequency $k_F = \omega_F c/U_F$.

The flutter speed, U_F, and frequency, ω_F, will then follow from equation (5) which can be written as

$$\frac{d\tilde{C}_{MR}}{d\tilde{\alpha}} = \left(\frac{2K}{\rho c^2}\right)\frac{1}{U^2} - 2I_o\mu k^2 \qquad (9)$$

where μ is the mass ratio $\mu = \rho_s t/\rho c$ and I_o is a dimensionless moment of inertia for the foil $(I = I_o \rho_s t c^3)$. At $k = k_F$ this yields $U = U_F$ given $I_o\mu$, $2K/\rho c^2$, and the value of the L.H.S. at $k = k_F$.

Consider first the case of subsonic, non-cavitating and non-separating flow examined by Smilg (1949) using Theodorsen's linearized unsteady airfoil theory. Smilg found that single degree of freedom flutter could only occur when the hinge was located between the leading edge and the quarter chord point $(0 < \beta < 0.25)$; otherwise $d\tilde{C}_{MI}/d\tilde{\alpha}$ was negative for all non-zero values of k. Even within the range $0 < \beta < 0.25$ single degree of freedom flutter could only occur for foils with very large mass ratios. Consequently single degree of freedom flutter will not occur for practical foils such as those employed in the present experiments. However in the non-cavitating tests discussed earlier the flow was clearly separating from the leading edge and forming a wake. It might be suggested that the dynamics under these circumstances would be more akin to those of the cavitating flow as anticipated by Woods (1957). The present tests did not support this view since the cavitating foils fluttered yet there was no evidence of flutter in non-cavitating flow at speeds as much as 50% greater than the cavitating foil flutter speed. The reason for this discrepancy is not entirely clear but is probably due to the differences in the dynamic response of free shear layers and cavity free surfaces.

Turning now to the case of cavitating flow we shall restrict our theoretical analysis to the simplest case of infinitely long cavities in an

unbounded flow (for which $\sigma = 0$). One of the reasons for this restriction is the difficulty involved in finding satisfactory closure models for the cavity in unsteady flow. Certainly none of the available models come close to representing properly the real events we have described occurring in the closure region. The unsteady lift and moment coefficients for the case of infinitely long cavities were evaluated first by Woods (1957) and Parkin (1957). Later the linearized theory for small angles of attack was further developed by Martin (1962) and Parkin (1962). In addition Kelly (1967) has extended Woods' (1957) results to larger angles of attack and finite cavities ($\sigma > 0$). For present purposes we shall employ Martin and Parkin's linearized results which yield a moment coefficient about the hinge point given by

$$\frac{2}{\pi}\frac{dC_M}{d\tilde{\alpha}} = -\frac{5}{16}\left\{\Omega(k) + \frac{5}{8}jk - \frac{245}{512}k^2\right\} + \beta\left\{\Omega(k) + \frac{5}{16}jkW(k) - \frac{35}{64}k^2\right\}$$

$$-\beta^2\left\{jkW(k) - \frac{9}{16}k^2\right\} \qquad (10)$$

where $\Omega(k)$, $W(k)$ are complex functions tabulated by Parkin (1962). A polar plot is presented in figure 26 for various locations of the hinge point, β; values of k are indicated on the curves. Note that in direct contrast to the Smilg case the flow with an infinite cavity <u>will</u> exhibit single degree of freedom flutter if the effective hinge point is anywhere between about mid-chord and the trailing edge ($\beta = 1$). The critical or flutter reduced frequency, k_F, for which $d\tilde{C}_{MI}/d\tilde{\alpha} = 0$ is plotted against the hinge position, β, in figure 27; also shown is the corresponding value of $d\tilde{C}_{MR}/d\tilde{\alpha}$ at $k = k_F$. It remains to determine whether single degree of freedom flutter or divergence will occur by comparing the flutter speed,

U_F, with the divergence speed, U_D. From equations (7) and (9) it is clear that

$$\frac{U_F^2}{U_D^2} = \left(\frac{dC_{MR}}{d\tilde{\alpha}}\right)_{k=0} \Bigg/ \left[\left(\frac{dC_{MR}}{d\tilde{\alpha}}\right)_{k=k_F} + 2I_o\mu k_F^2\right] \tag{11}$$

From the expression (10),

$$\left(\frac{d\tilde{C}_{MR}}{d\tilde{\alpha}}\right)_{k=0} = \frac{\pi}{2}\left(\beta - \frac{5}{16}\right) \tag{12}$$

and this is included in figure 27. Consequently the flutter speed is virtually always less than the divergence speed, irrespective of $I_0\mu$. Indeed the foil will exhibit single degree of freedom flutter at speeds far below the divergence speed as demonstrated by the values of U_F/U_D plotted in figure 28 for various hinge point locations and values of $I_0\mu$. Furthermore the flutter frequency, ω_F, is readily related to the natural frequency of the foil in a flow at speeds much smaller than the flutter speed (denoted by ω_N) by

$$\frac{\omega_F}{\omega_N} = \left[\left\{\left(\frac{1}{k^2}\frac{d\tilde{C}_{MR}}{d\tilde{\alpha}}\right)_{k\to\infty} + 2I_o\mu\right\} \Bigg/ \left\{\left(\frac{1}{k^2}\frac{d\tilde{C}_{MR}}{d\tilde{\alpha}}\right)_{k=k_F} + 2I_o\mu\right\}\right]^{\frac{1}{2}} \tag{13}$$

As seen by the plots included in figure 28 ω_F/ω_N for small values of $I_0\mu$ is virtually always between 0.85 and 0.9 and tends toward 1.0 for very large $I_o\mu$.

It is surprising that this unique feature of supercavitating foil dynamics has received little attention in previous studies, despite the fact that it was briefly alluded to by Woods (1957) in his pioneering calculations of the unsteady lift and moment coefficients. What makes it more

surprising is the fact that most supercavitating foils with wedge-like thickness distributions will have an elastic axis at a distance about 2c/3 from the leading edge and hence will be susceptible to single degree of freedom flutter. Kaplan and Henry (1960) and Song (1972) both performed conventional two degree of freedom wing flutter analyses for supercavitating hydrofoils without mentioning the simpler instability. The experiments of Kaplan and Lehman (1966), Song and Almo (1967) and Cieslowski and Pattison (1965) all utilized systems with elastic axes forward of midchord and are therefore relevant only to the possibility of the conventional wing flutter which could arise under these circumstances. We have not been able to identify any other experimental results for the more practical supercavitating foil case in which the elastic axis is aft of midchord.

The experimental reduced flutter speeds for long cavities (see figure 11) are in the range 0.15 to 0.25 corresponding to a range of reduced frequencies, k_F, from 7 to 4. These are in fair agreement with the theoretical results for a model hinged at the trailing edge for which $k_F = 7$. One might argue that it is more appropriate to use a theoretical model whose chord is equal to the flexible chord, a, in the experiments. However, this yields theoretical k_F values of about 12 which are even further from the 4→7 range observed experimentally. It should however be appreciated that the model is rather crude and that the oscillatory camber which is absent in the model may have significant dynamic effects. Recently Murai (1978) and Shimuzu (1979) have computed reduced flutter frequencies for various shapes of foils rigidly supported at their trailing edge. Figure 29 has been constructed from their results and presents the reduced flutter frequency as a function of parametric shapes varying from

a flat plate to a wedge. The flat plate yields $k_F = 12$ which is qualitatively consistent with our simpler model but significantly larger than the experimental observations.

The experimental observation of a minimum flutter speed at an angle of attack of about 10^o cannot, of course, be predicted by a linear theory whose results are independent of α_o. It is interesting to note that Kelly's (1967) non-linear calculations at $\alpha_o = 0$, 10 , 20 , and 30^o reveal some instances in which the coefficients exhibit extremums at 10^o. However more pertinent evaluation of polar plots like those of figure 26 using Kelly's tables indicated that though the values of $d\tilde{C}_{MI}/d\tilde{\alpha}$ increased considerably with α_o neither the value of k_F nor the value of $(d\tilde{C}_{MR}/d\tilde{\alpha})_{k=k_F}$ were substantially different from those given in figure 27.

Kelly's results can also be used to assess the effect of cavity length since he calculated coefficients for cavitation numbers greater than zero (0.3, 0.6 and 0.9). In general the shorter cavities yield marginally smaller values for k_F . Superficially this is consistent with the experimental trend. However we believe that the cavity closure dynamics discussed in Section 7 cause substantially alterations in the flutter dynamics for short cavities. None of the theoretical models adequately incorporate these observed closure phenomena.

Some other interesting trends emerge from a comparison of experimentally measured lift and moment coefficients with those predicted by the theory. DeLong and Acosta (1969) measured coefficients for supercavitating hydrofoils performing heave motions only and found that both in-phase and quadrat lift coefficients (which would contribute to $d\tilde{C}_{MR}/d\tilde{\alpha}$ and $d\tilde{C}_{MI}/d\tilde{\alpha}$ in our notation) were both in general less than the theoretical values. One could conclude that the resulting experimental k_F would be less than the theory which is consistent with the results of this investigation.

Furthermore Klose and Acosta (1969) found that ventilated, air-filled cavities exhibited significant cavity pressure variations. This could account for the fact that their measured in-phase lift coefficients were much larger than the theory and their quadrature coefficients were comparable with the theory. Comparison with De Long and Acosta's results suggests significant differences between the coefficients for ventilated and natural cavities. In the present tests the air-filled cavities examined in the FSWT tests manifest substantially lower reduced flutter velocities (about 0.11) than the natural cavities in the HSWT tests.

It was also shown in figure 28 that the theoretical flutter frequency, ω_F, should only be slightly smaller than the natural frequency, ω_N, in flows with velocity well below the flutter velocity. This was borne out by the experimental results of figure 5 which suggests a flutter frequency which is no more than 10% less than ω_N. Furthermore the experiments indicated that ω_N was close to the natural frequency of the foils in still water ω_W (see Tables). This quantity ω_W may however be difficult to estimate theoretically as discussed in Section 3.

Given k_F and ω_F the flutter speed, U_F, follows from $U_F = \omega_F c/k_F$. A comparison between the calculated and observed flutter speeds is essentially contained within the comparison of the k_F values.

Finally it is necessary to discuss the nature of leading edge flutter as defined in the introduction. It should now be clear that a practical supercavitating foil rigidly supported at one end with its elastic axis aft of the midchord and with a slender leading edge is suspectible to several different instabilities. One can for example identify a simple torsional instability for which the results of the last section are directly applicable. There is also the possibility of leading edge flutter which involves chordwise bending and large amplitudes at the slender leading edge. The flutter speed for each of these will presumably be governed by $U_F^* = \omega_F^* c^*/k_F^*$

where ω_F^* is the natural underwater frequency in that mode, c^* is an "effective" chord length ($c^* = c$ for torsional instability but less for leading edge flutter) and k_F^* is the appropriate critical constant for each instability. Now ω_F^* would normally be greater for the leading edge flutter mode than for torsional instability. However c^* is less for the former; consequently it is not immediately obvious which instability will have the lower flutter speed. In this respect it is of interest to review the two cases (Waid and Lindberg (1957) and Spangler (1966)) mentioned in the introduction. According to figure 27 the lowest torsional flutter speed is given by $k_F = 17$. If the cavity surface waves are convected at U_F^* then this leads to a cavity surface wavelength, λ, to chord ratio of $\lambda/c = 0.3$. On the other hand if we estimate leading edge flutter to occur when $\omega_F^* c^*/U_F \approx 3$ ($c^* \cong a$ = effective flexible chord) then $\lambda/c^* \cong 2$. Now the photographs of Waid and Lindberg (1957) and Spangler (1966) indicate c/λ values of about 4 and 8 respectively. This suggests that leading edge flutter was predominant in both cases with effective flexible chord lengths of $c/8$ and $c/16$ respectively.

The present report has concentrated on a fundamental investigation of leading edge flutter and has conclusively demonstrated the existence of the phenomenon. The experimental models were designed to have relatively simple modes of vibration and it has been demonstrated that once these underwater modes and natural frequencies are known reasonable estimates can be made of the leading edge flutter speed. Furthermore a rather simple theoretical model yields values of the critical reduced velocity, $1/k_F$, which are within a factor of two of the observations and could be used as a conservative design estimates since they are lower than those observed experimentally.

ACKNOWLEDGEMENTS

The authors are very grateful to a number of people whose help and guidance was invaluable. Discussions with A. J. Acosta and T. Y. Wu were greatly appreciated. Help given by T. Ward, J. Kingan, H. Gabler, H. Hamaguchi, V. Sodha and C. Hemphill is gratefully acknowledged. Finally we are most appreciate of the support provided by Naval Sea Systems Command General Hydromechanics Research Program administered by the David Taylor Naval Research and Development Center under Contract No. N00014-75-C-0379 for which this serves as the final report.

REFERENCES

1. Abramson, H. N., 1969, Hydroelasticity: A review of hydrofoil flutter. Appl. Mech. Reviews, Vol. 22, No. 2, pp. 115-121.

2. Acosta, A. J., 1973. Hydrofoils and hydrofoil craft. Annual Reviews of Fluid Mechanics, Vol. 5, pp. 161-184.

3. Barton, M. V., 1951. Vibration of rectangular and skew cantilever plates. J. Appl. Mech., Vol. 18, No. 2, pp. 129-134.

4. Cieslowski, D.S. and Pattison, J.H., 1965. Unsteady hydrodynamic loads and flutter of two-dimensional hydrofoils. Hydrofoil Symposium, SNAME, Paper No. 2-b (Also published as: Cieslowski, D.S. 1965. Flutter of a two-dimensional two-degree-of-freedom hydrofoil. NSRDC Test Rep. No. 051-H-01, Feb. 1965).

5. DeLong, R.K. and Acosta, A. J., 1969. Experimental investigation of non-steady forces on hydrofoils oscillating in heave. C.I.T. Engineering Division Report, March 1969.

6. English, J., Ship Division, National Physical Laboratory, England, personal communication, 1978.

7. Gross, L., NASA George Marshall Space Flight Center, Huntsville, Alabama, personal communication, 1975.

8. Kaplan, P. and Henry, C. J., 1960. A study of the hydroelastic instabilities of supercavitating hydrofoils. J. Ship Res., Vol. 4, No. 3, pp. 28-38.

9. Kaplan, P. and Lehman, A. F., 1966. An experimental study of hydroelastic instabilities of finite span hydrofoils under cavitating conditions. AIAA J. Aircraft, Vol. 3, pp. 262-269.

10. Kelly, H.R., 1967. An extension of the Woods theory for unsteady cavity flows. ASME J. Basic Eng., Vol, 89, No. 4, pp. 798-806.

11. Klose, G.J. and Acosta, A.J., 1969. Unsteady force measurements on superventilated hydrofoils in heaving motion. J. Ship Res., Vol. 13, No. 2, pp. 92-102.

12. Lindholm, U.S., Kana, D.D., Chu, W.H. and Abramson, H.N., 1965. Elastic vibration characteristics of cantilever plates in water. J. Ship Res., Vol. 9, No. 1, pp. 11-36.

13. Martin, M., 1962. Unsteady lift and moment on a fully cavitating hydrofoil at zero cavitation number. J. Ship Res., Vol. 6, No. 1 pp. 15-25.

14. Murai, H., 1978. Theoretical study of a flexible supercavitating hydrofoil. Japanese Society of Mechanical Engineering 91st Conference. Paper No. 218 (in Japanese), pp. 211-213.

15. Osterwalder, J. and Sonsino, M. 1975. Investigations concerning natural vibrations and flow induced vibrations on Kaplan turbine runner blades. Proc. 5th conference on Fluid Machinery, Budapest, Hungary; Akademioi Kiado, Budapest, 1975.

16. Parkin, B.R., 1957. Fully cavitating hydrofoils in nonsteady motion. CIT Engineering Report No. 85-2, 1957.

17. Parkin, B.R., 1962. Numerical data on hydrofoil response to nonsteady motions at zero cavitation number. J. Ship Res., Vol. 6, No. 3 pp. 40-42.

18. Rothblum, R.S., Mayer, D.A. and Wilburn, G.M., 1969. Ventilation, cavitation and other characteristics of high speed surface piercing struts. Naval Ship Research and Development Center Report No. 3023.

19. Smilg, B., 1949. The instability of pitching oscillation of an airfoil in subsonic incompressible potential flow. J. Aero. Sci., Vol. 16, No. 11, pp. 691-696.

20. Shimizu, S., Institute of High Speed Mechanics, Tohuku University, Sendai, Japan, personal communication, 1979.

21. Song, C.S. and Almo, J., 1967. An experimental study of the hydro-elastic instability of supercavitating hydrofoils. St. Anthony Falls Hydraulic Lab Project Report No. 89, Univ. of Minnesota.

22. Song, C.S., 1972. Flutter of supercavitating hydrofoils - comparison of theory and experiment. J. Ship, Res., Vol. 16, No. 3, pp. 153-166.

23. Spangler, P.K., 1966. Performance and correlation studies of Bu Ships parent hydrofoil at speeds from 40 to 75 knots. Naval Ship. Res. Dev. Cen. Rep. No. 2353.

24. Waid, R. L. and Lindberg, L. M., 1957. Experimental and theoretical investigations of supercavitating hydrofoil. California Institute of Technology, Engineering Division Report No. 47-8, April 1957.

25. Ward, T. M., 1976. Report on water tunnel tests of three hydrofoils having very sharp leading edges in fully wetted and cavitating flows. Galcit Report, HSWT-1124, California Institute of Technology.

26. Woods, L. C., 1957. Aerodynamic forces on an oscillating aerofoil fitted with a spoiler., Proc. Roy. Soc., Series A. Vol 239, pp. 328-337.

27. Young, J. O. and Holl, J. W., 1966. Effects of cavitation on periodic wakes behind symmetric wedges. ASME J. Basic., Eng., Vol. 88, No. 1, pp. 163-176.

TABLE 1. DATA ON 35.5cm. SPAN FOILS

FOIL NO.	THICKNESS t(mm.)	MASS RATIO $\mu^*=\rho_s t/\rho a$	FIRST MODE FREQ. (HZ.) IN AIR $\omega_A/2\pi$	FIRST MODE FREQ. (HZ.) IN "STILL" WATER $\omega_W/2\pi$	SECOND MODE FREQ. (HZ.) IN AIR	SECOND MODE FREQ. (HZ.) IN "STILL" WATER	DIVERGENCE SPEED	FLUTTER FREQ. (HZ.) $\omega_F/2\pi$	FLUTTER SPEED (M/SEC) U_F	$U_F/\omega_F c$
F16	.406	.012	37.0	6.3			1.2	****	****	****
			(35)*	(2.2)+	(42)*	(4.3)+	(1.16)** (1.62)++			
F31	.787	.024	69.0	14.0		19.2	2.1	12	<1.2+++	<0.106
			(67)*	(5.9)+	(82)*	(11.5)+	(3.2)** (4.4)++			
F61	1.55	.047		37.5		50.5	***	38	≈4	0.109
			(132)*	(16.1)+	(160)*	(31)+	(8.9)** (12.0)++			
F89	2.26	.069	230.4	62.5	267	89.0	***	65	≈7	0.113
			(193)*	(28.2)+	(234)*	(55)+	(15.6)** (21.3)++			

* Theoretical values using Barton's (1951) method

\+ Theoretical values using Lindholm, Kana, Chu and Abramson's (1965) method

** Non-separated flow theoretical value (see Appendix C)

++ Cavitating or wake flow theoretical value (see Appendix C)

*** Velocity not attainable in present experiments

+++ Unbounded flutter occurred at the lowest speed at which a cavity could be formed

**** Non-cavitating divergence occurred before a cavity could be formed.

NOTE: All foils have a/c ratio of 0.583 with chord c = 15.2cm.

TABLE 2. DATA ON 15.2cm. SPAN FOILS

FOIL NO.	THICKNESS t (mm.)	FLEXIBLE/ TOTAL CHORD (a/c)	MASS RATIO $\mu^*=\rho_s t/\rho a$	FIRST MODE FREQ. (HZ.) IN AIR $\omega_A/2\pi$	FIRST MODE FREQ. (HZ.) IN "STILL" WATER $\omega_W/2\pi$	FLUTTER FREQ. (HZ.) $\omega_F/2\pi$	FLUTTER SPEEDS FOR LONG CAVITIES U_F(M/SEC) $\alpha=7^o$	$\alpha=10^o$	$\alpha=13^o$	$U_F/\omega_F c$ $\alpha=7^o$	$\alpha=10^o$	$\alpha=13^o$
H31	.787	0.583	.024	71.6 (67.2)*	(8.9)+							
H68	1.73	0.583	.052	159.3 (147.4)*	51.2 (25.6)+	44	<11			<0.26		
H89	2.26	0.583	.069	195.7 (192.9)*	71.2 (42.5)+	60	11.6	8.5	9.8	0.20	0.15	0.17
H125	3.17	0.583	.096	294.0 (270.4)*	95.8 (70.8)+	83	18.3	15.9	>18.3	0.23	0.20	>0.23
H50A	1.27	0.417	.054	192.3 (212.4)*	56.0 (35.5)+	53	<8.9			<0.175		
H125B	3.17	0.706	.080	200.0 (185.5)*	80.1 (48.0)+	60	11.5(8^o)	10.9	12.3	0.20(8^o)	0.19	0.215

* Theoretical values using Barton's (1951) method

\+ Theoretical values using Lindholm, Kana, Chu and Abramson's (1965) method

** Diverged and destroyed before a cavity could be formed

Note: All foils have a chord c=15.2

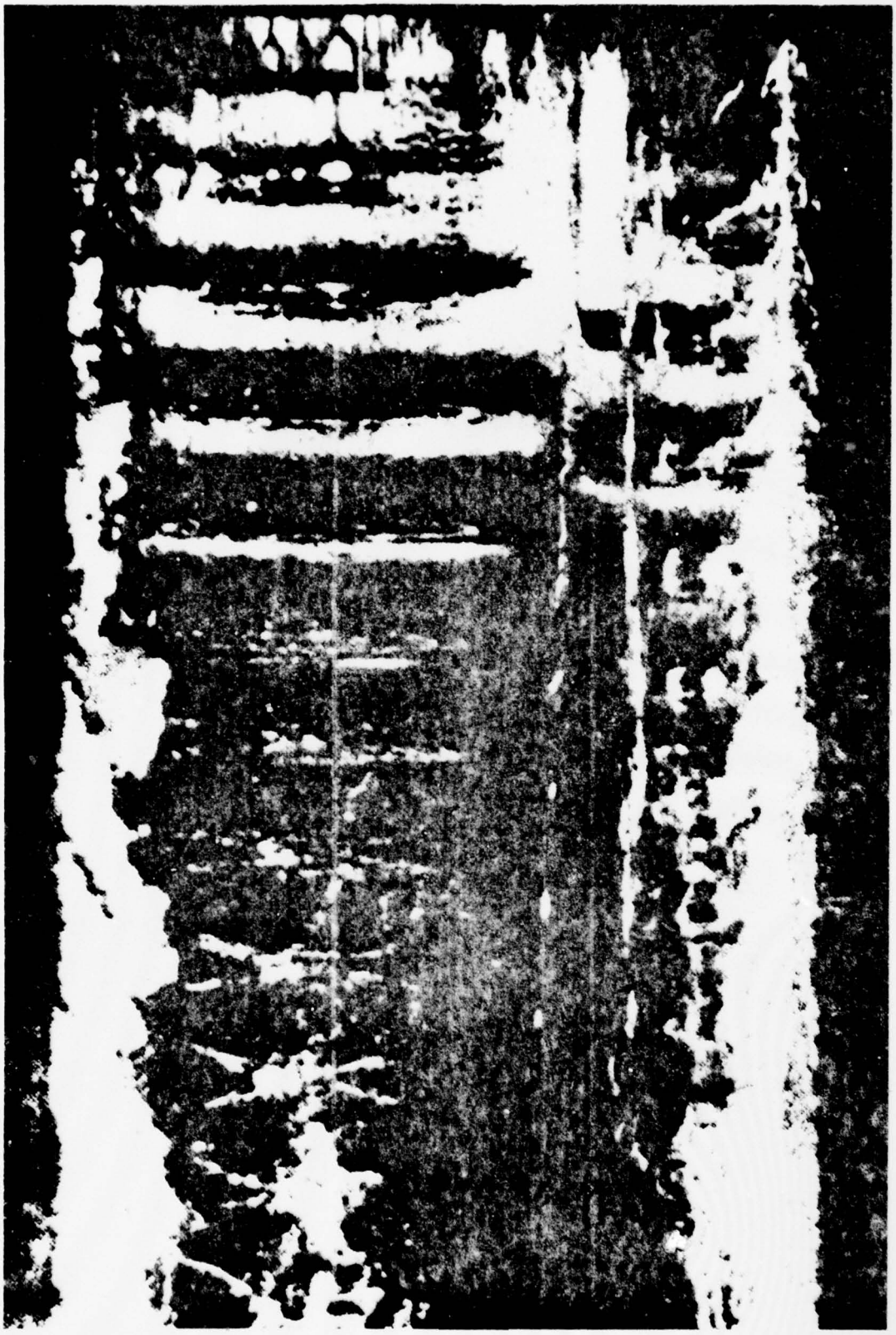

Figure 1. A photograph of the suction cavity surface taken by Waid and Lindberg (1957) during leading edge flutter ($\alpha = 5.7^{o}$, $\sigma = 0.12$; tunnel velocity of 8.9 m/sec; leading edge on extreme right).

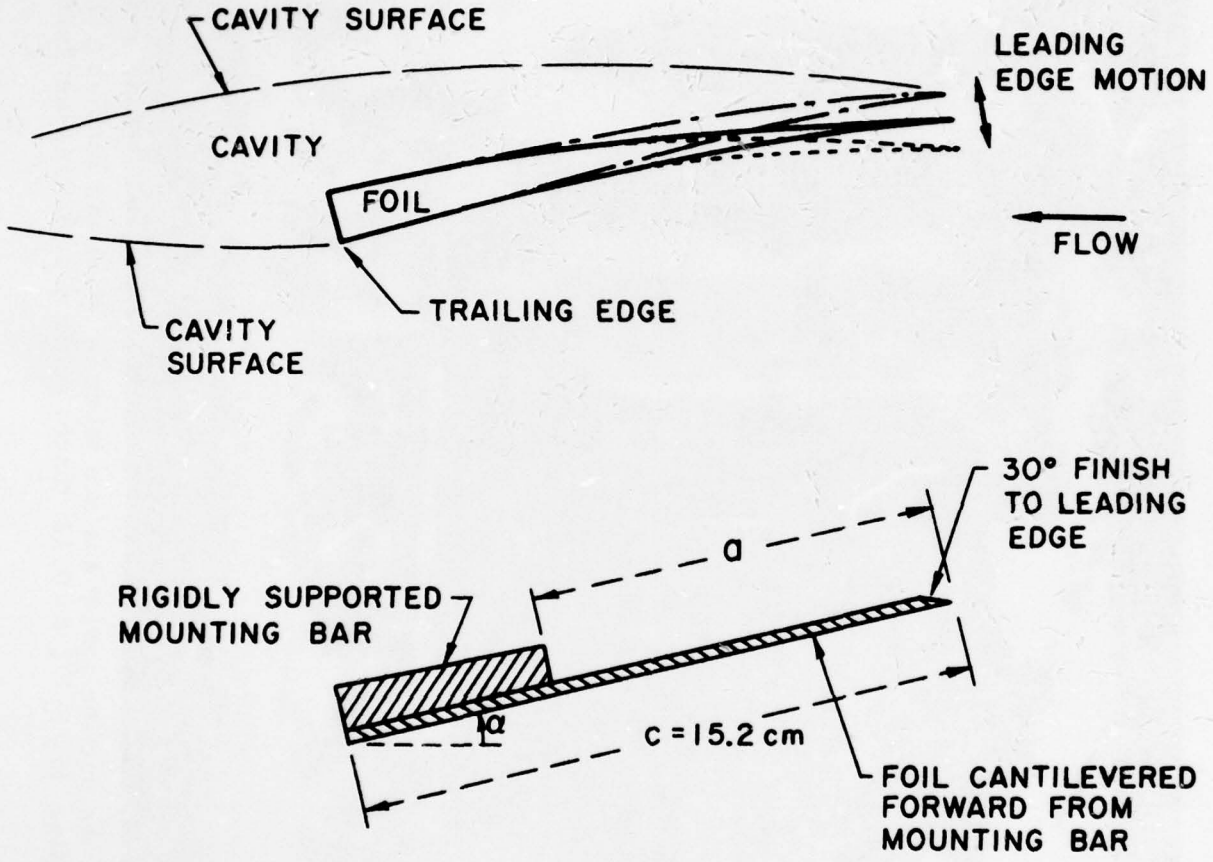

Figure 2. Above: typical supercavitating hydrofoils shape with the leading edge flutter mode and the cavity configuration sketched. Below: configuration of the models used in the experiments.

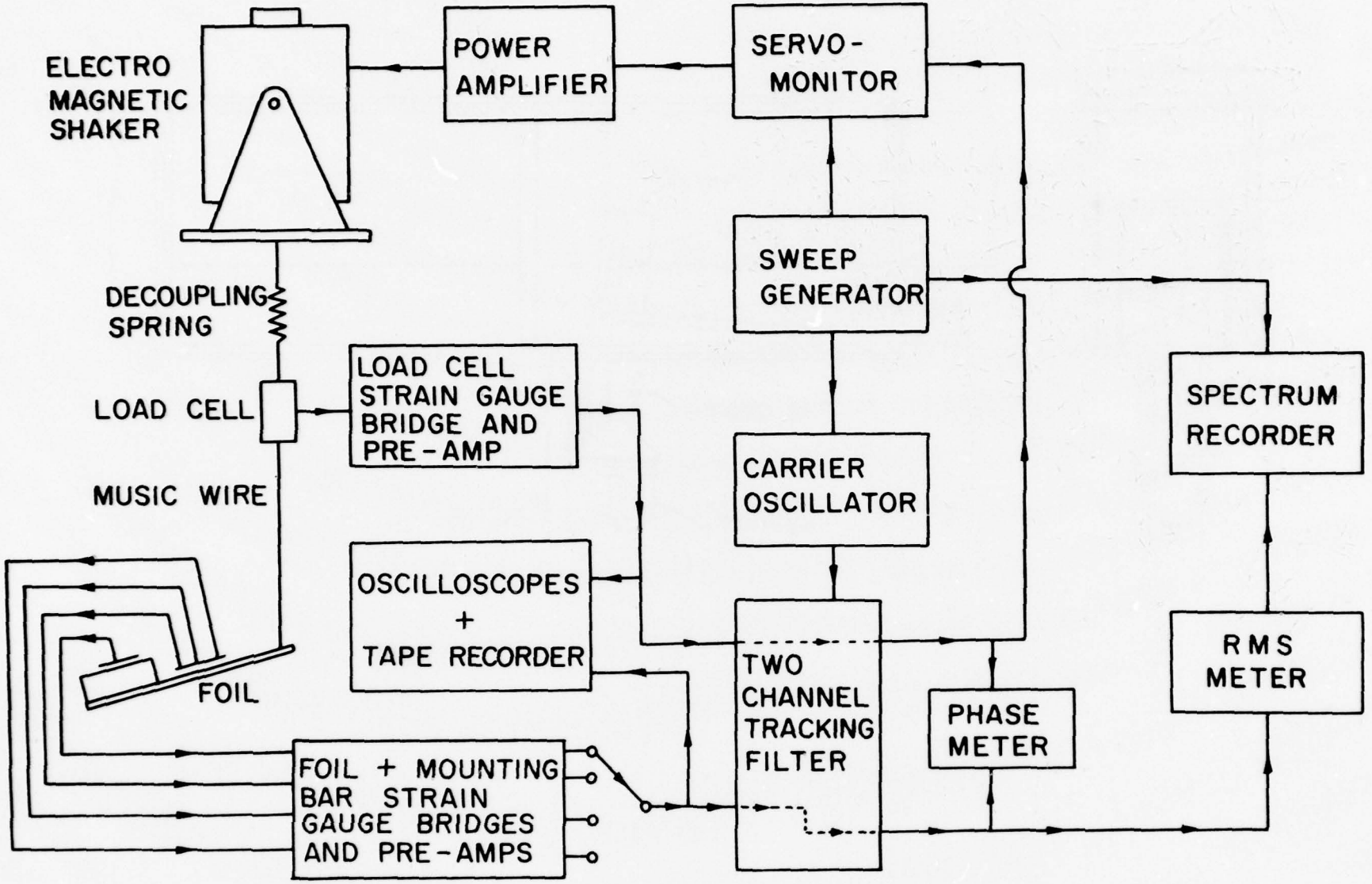

Figure 3. Block diagram of the electro-magnetic shaker excitation system and the signal processing.

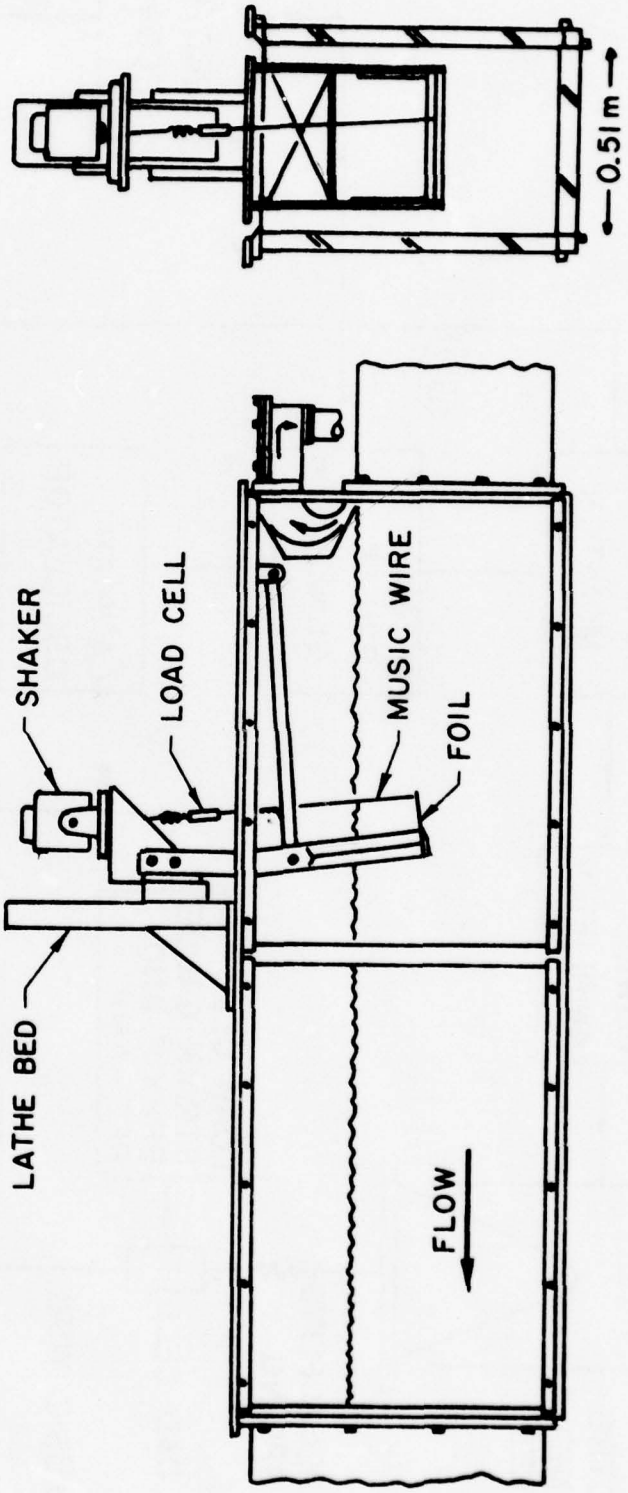

Figure 4. Mounting system for the 35.56 cm. span foils in the Free Surface Water Tunnel (FSWT).

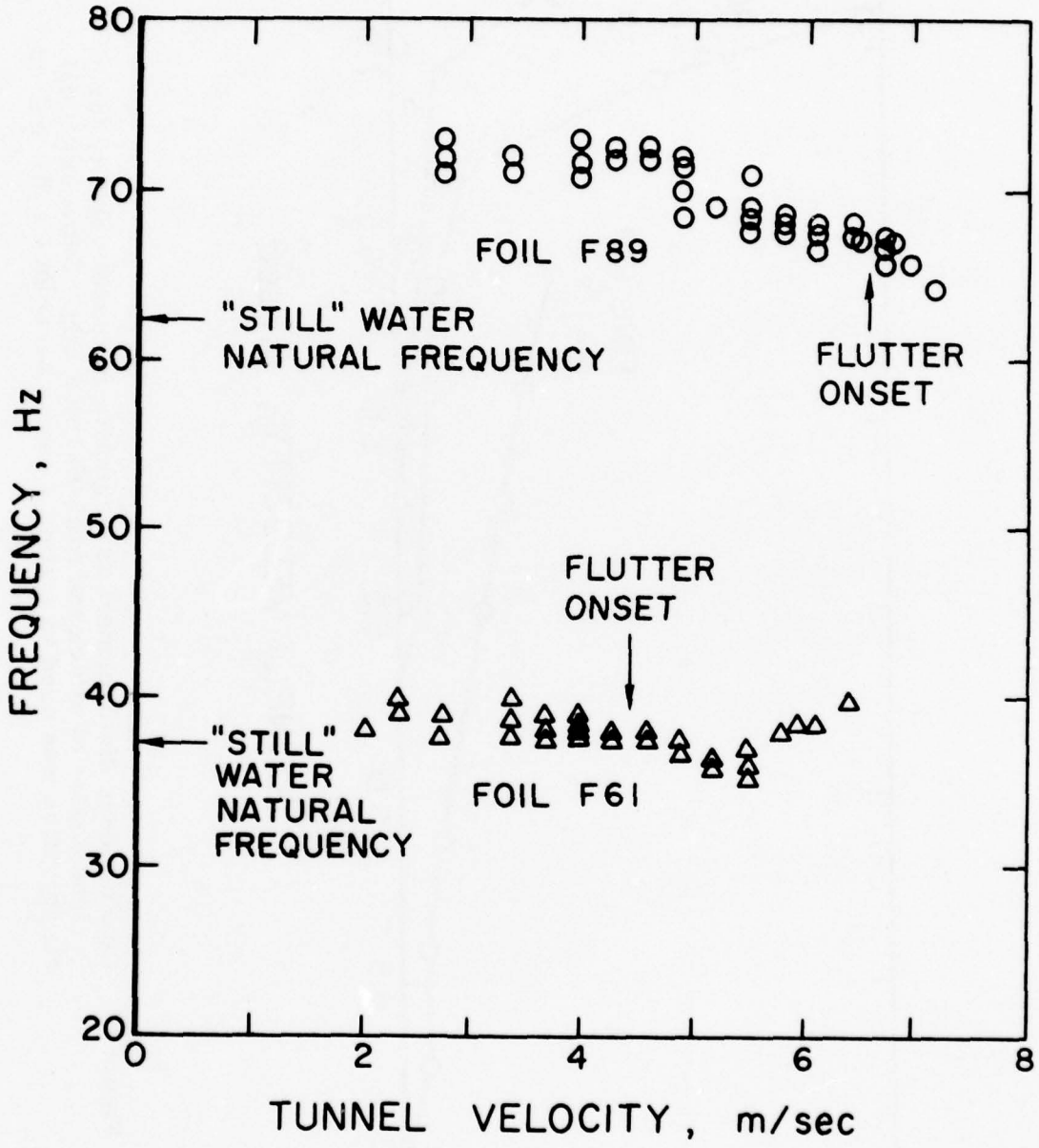

Figure 5. Natural frequencies for foils F61 and F89 as a function of tunnel velocity.

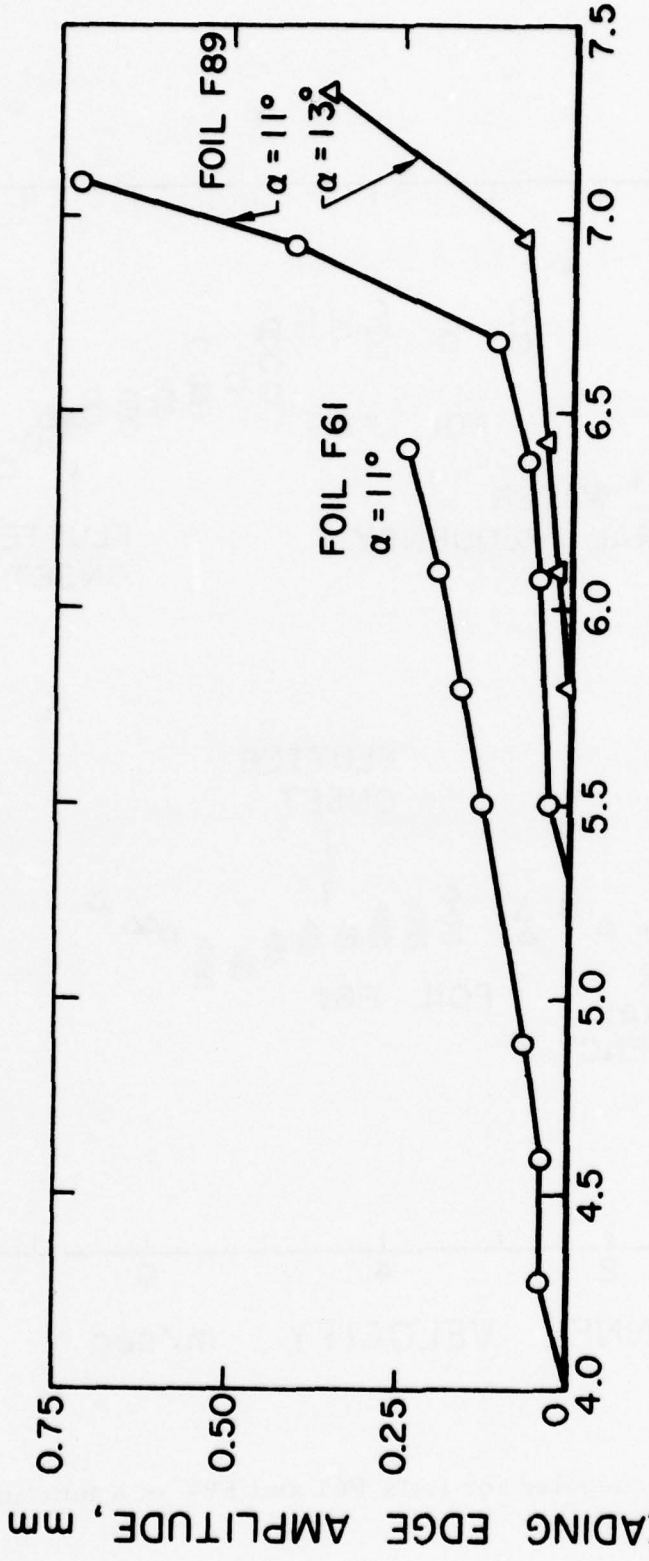

Figure 6. Leading edge displacement as a function of tunnel velocity for various angles of attack and foils F61 and F89. Some artificial air injection was used to sustain a cavity between 4 and 5 m/sec.

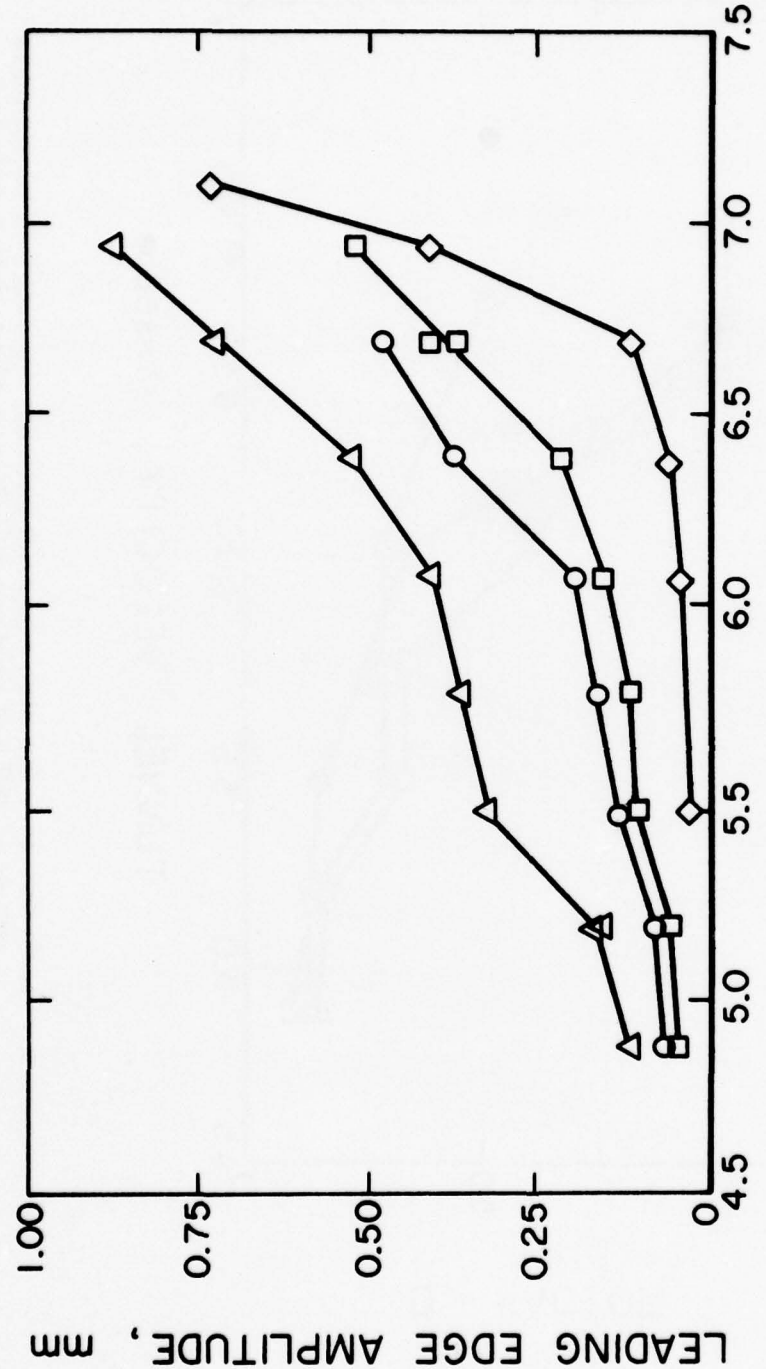

Figure 7. Leading edge displacement as a function of tunnel velocity for foil F89 at an angle of attack of 11° and various amplitudes of excitation force (◇ : no force, □ : 0.111 N, ○ : 0.222 N., △ : 0.444 N.)

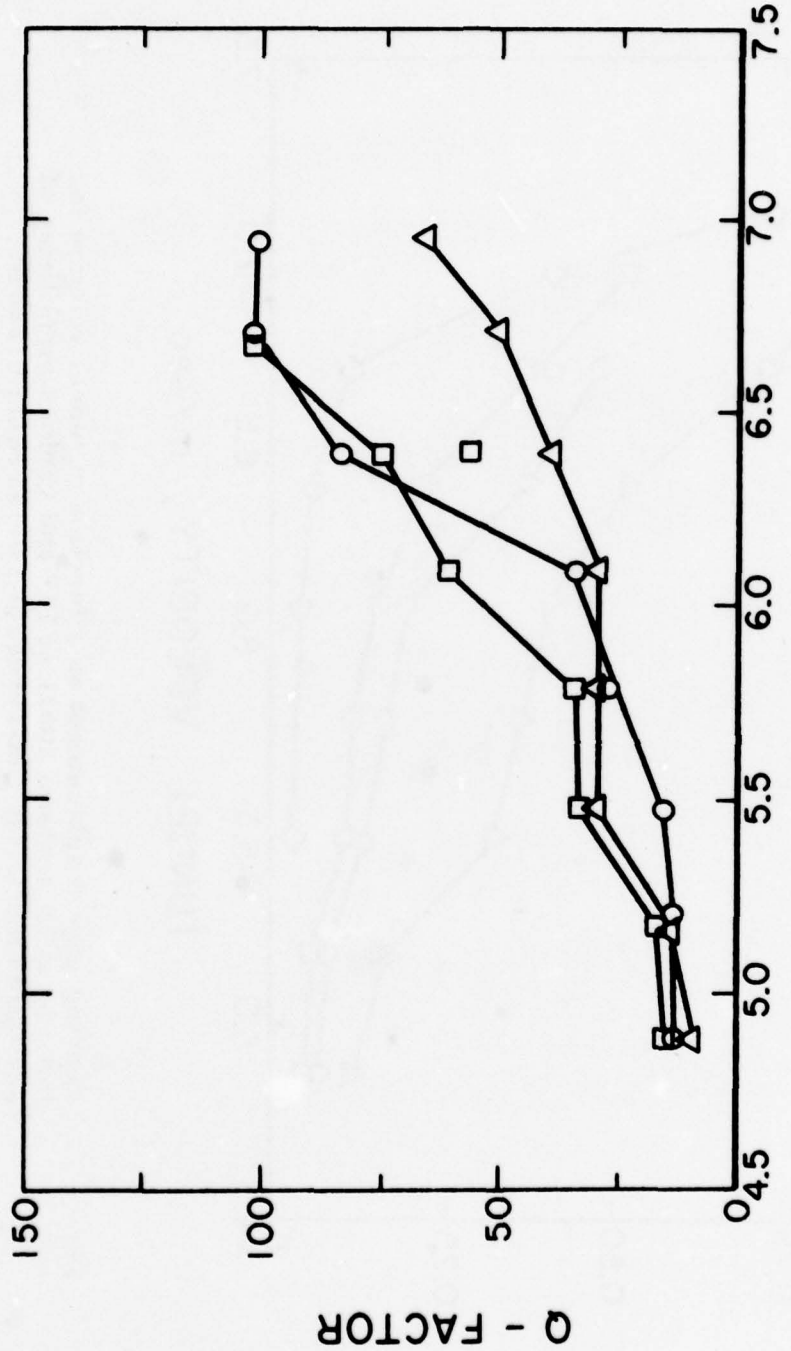

Figure 8. Q-factor as a function of tunnel velocity for foil F89 at an angle of attack of 11° and various amplitudes of excitation force as given in figure 7.

SIDE VIEW

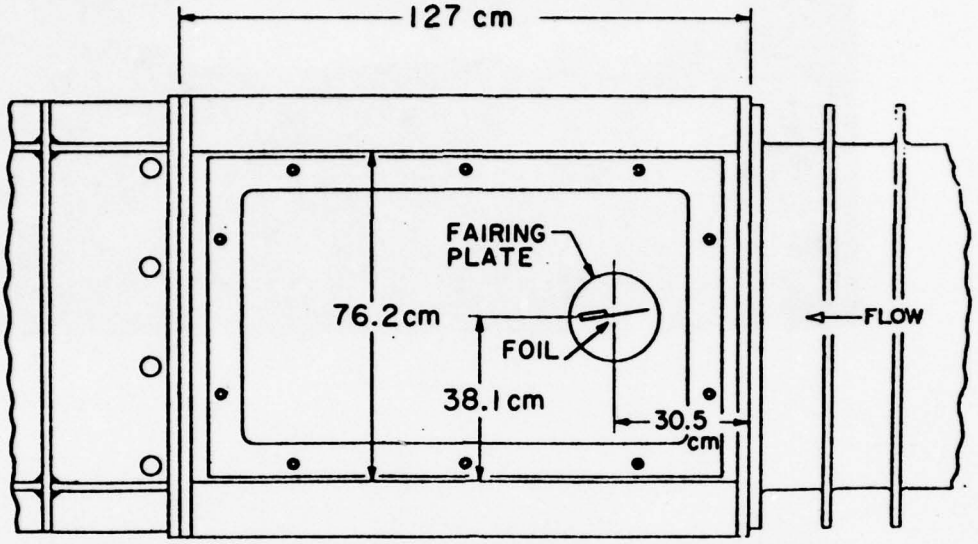

PLAN VIEW

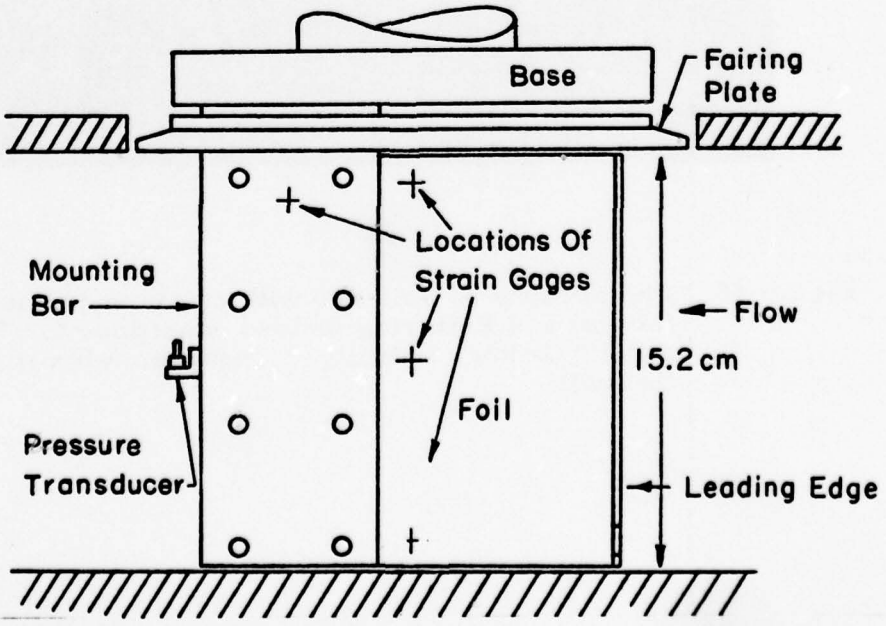

Figure 9. Mounting system for the 0.152 m. span foils in the High Speed Water Tunnel (HSWT).

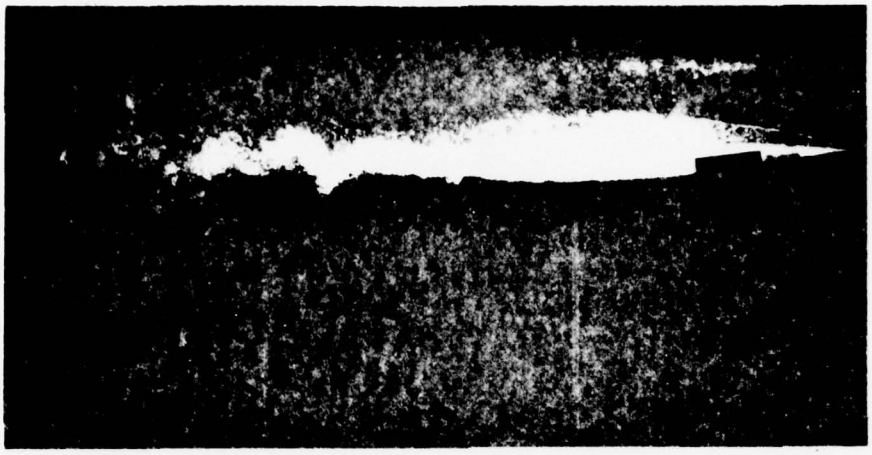

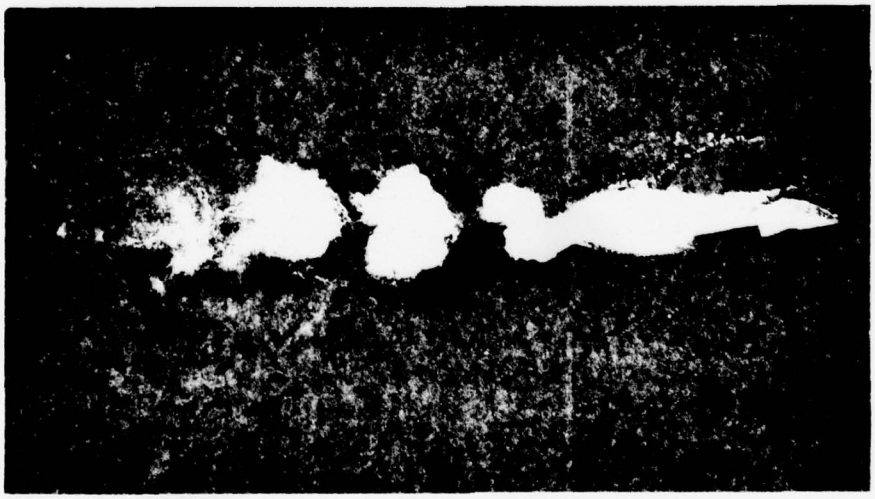

Figure 10. Photographs of Foil H89 with cavity under quiescent (above) and fluttering (below) conditions ($\alpha = 7^{o}$ (above) and 10^{o} (below); velocity = 6.6 m/sec (above) and 7.4 m/sec (below)).

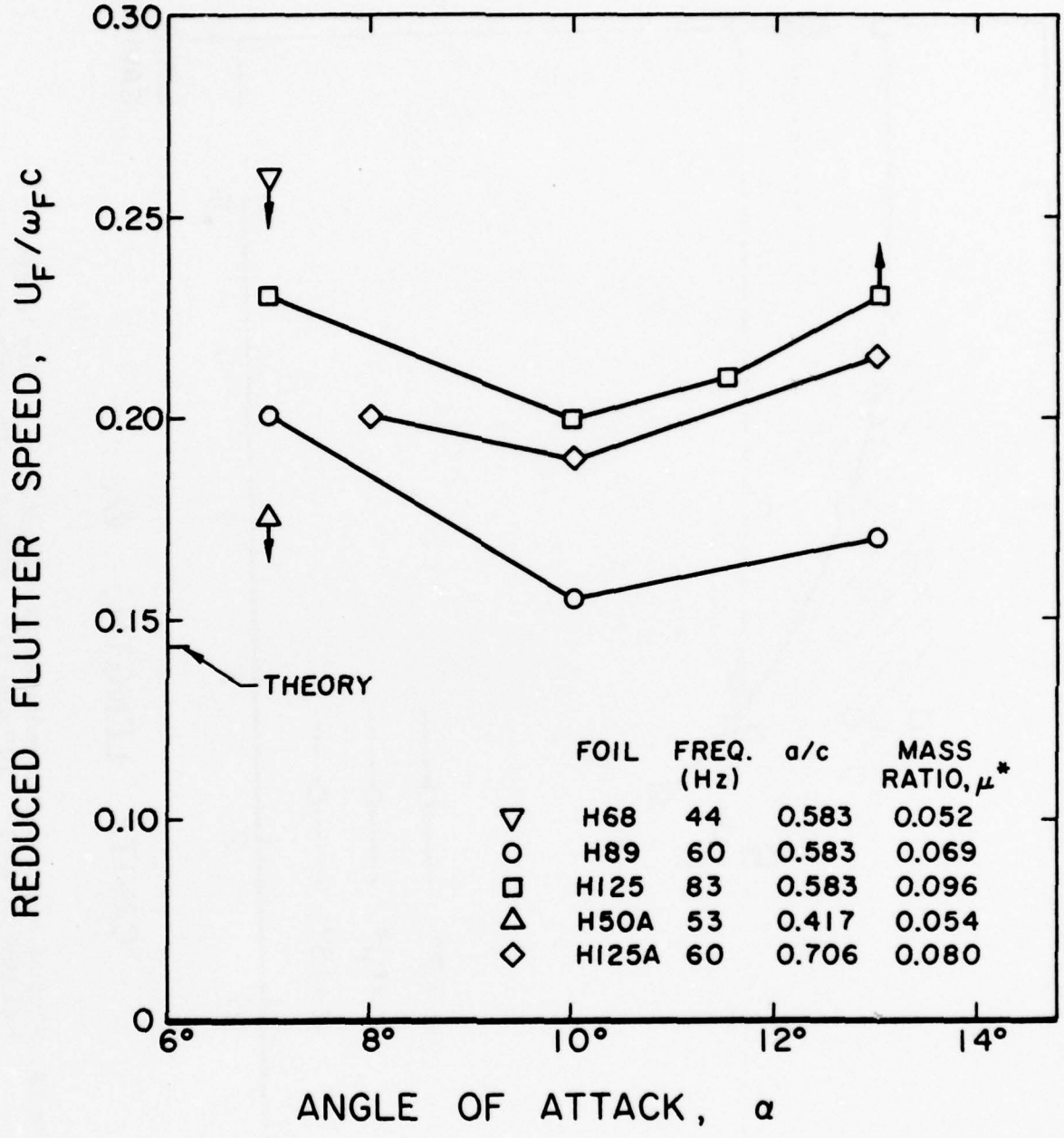

Figure 11. Reduced flutter speeds, $U_F/\omega_F c$, for long cavities as a function of angle of attack. The theoretical value of 0.143 is indicated on the vertical axis.

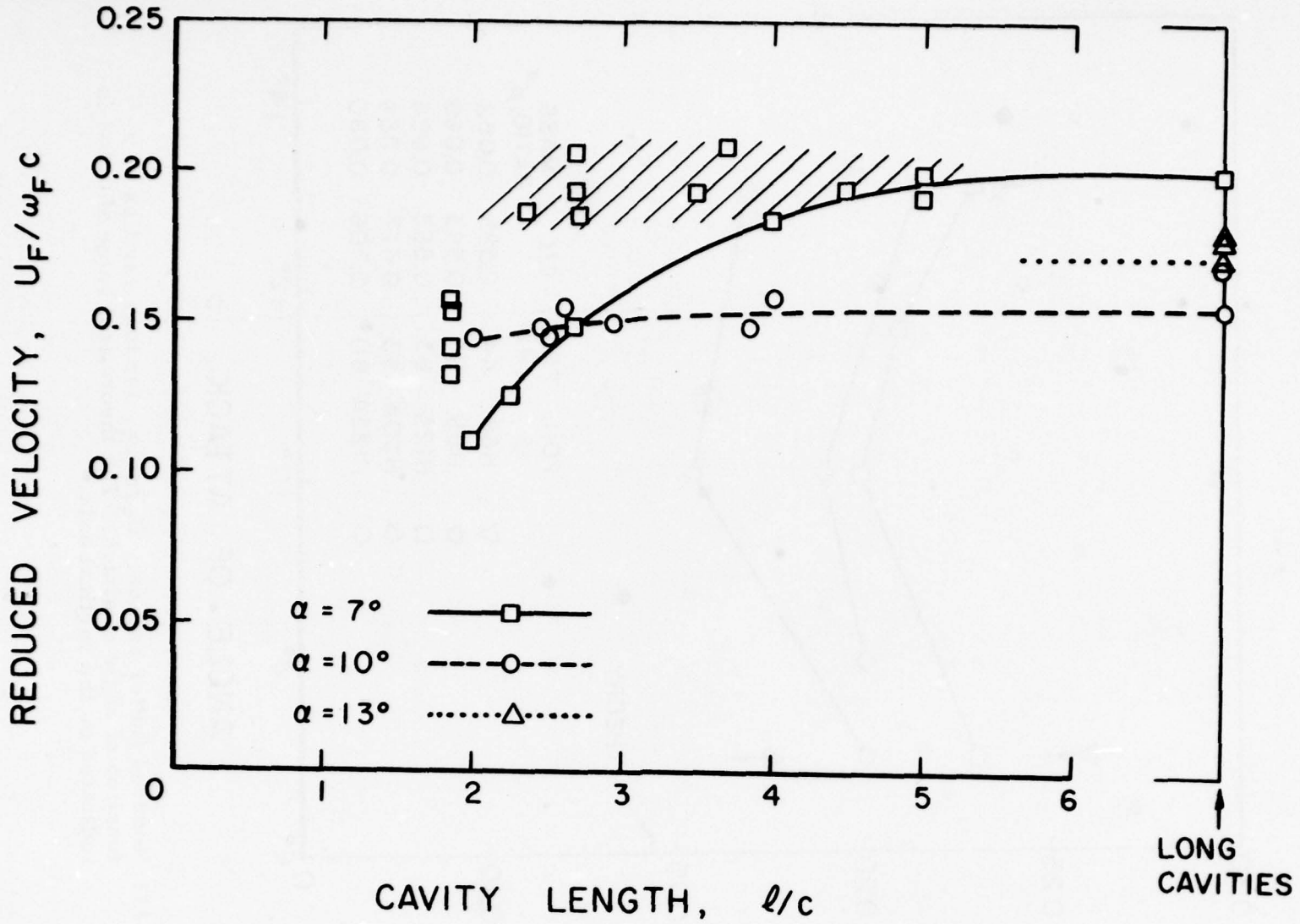

Figure 12. Flutter speed and boundaries as a function of cavity length for foil H89 at $\alpha = 7^{o}$, 10^{o} and 13^{o}. Values on the extreme right are for cavities which extended beyond the extent of the window in the working section. The hatched area and the points in it represent the regime of the resonant length phenomena.

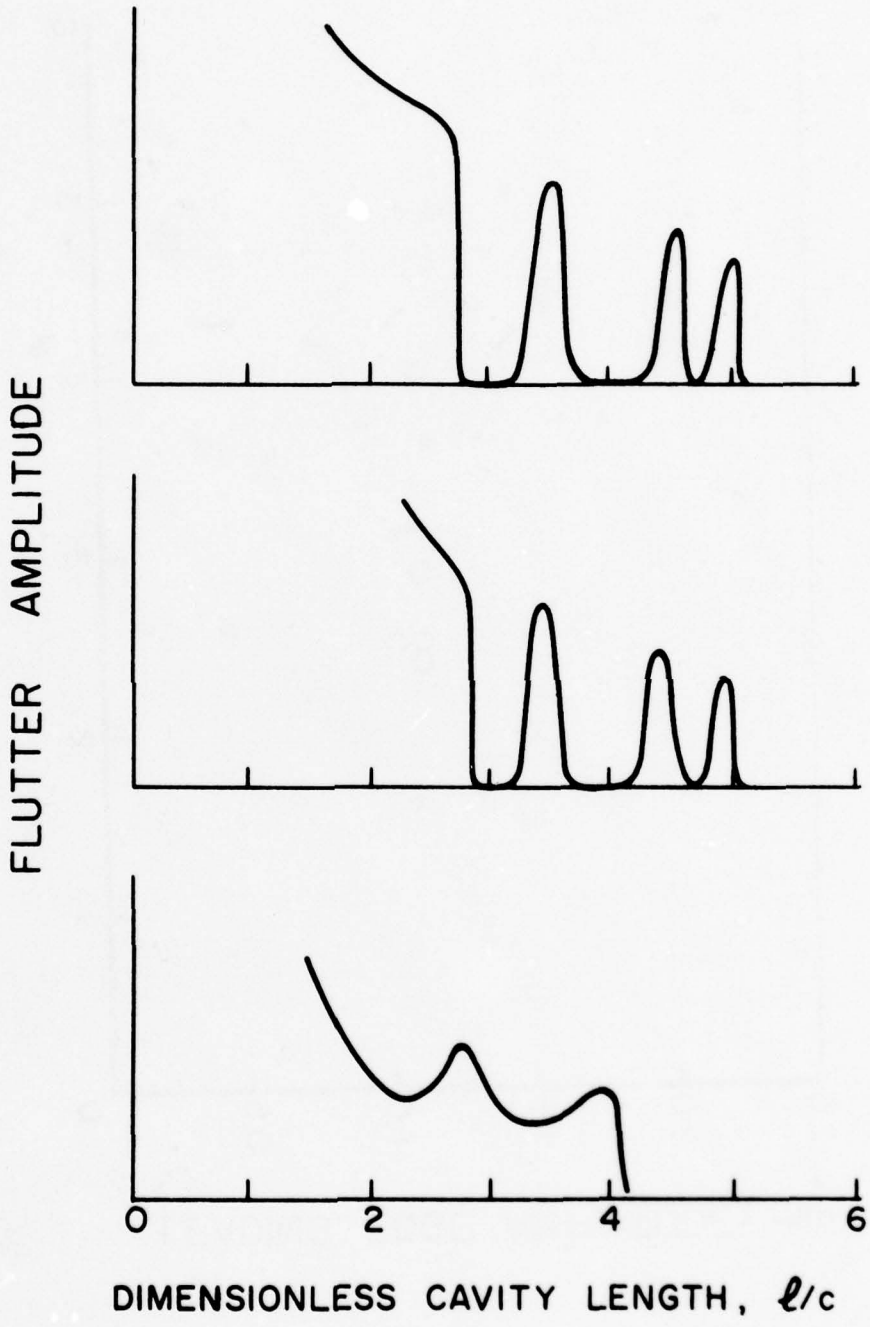

Figure 13. The resonant length phenomena illustrated in sketches of the flutter amplitude against the cavity length for foil H89 at $\alpha = 7^{\circ}$. The tunnel velocities are 11.9, 11.3 and 10.7 m/sec. from the top to the bottom.

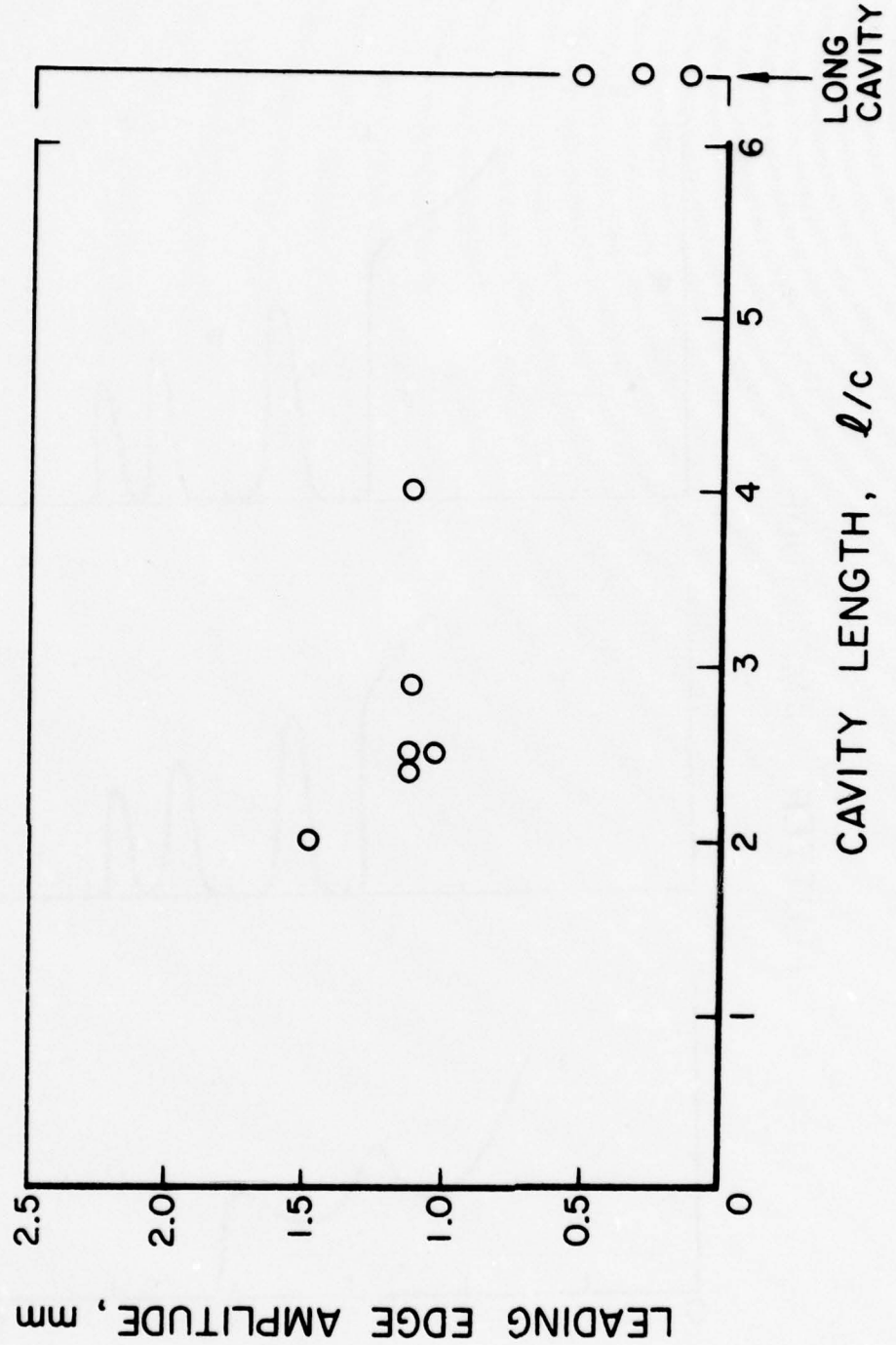

Figure 14. Leading edge amplitude versus cavity length for foil H89 at an angle of attack of 10°.

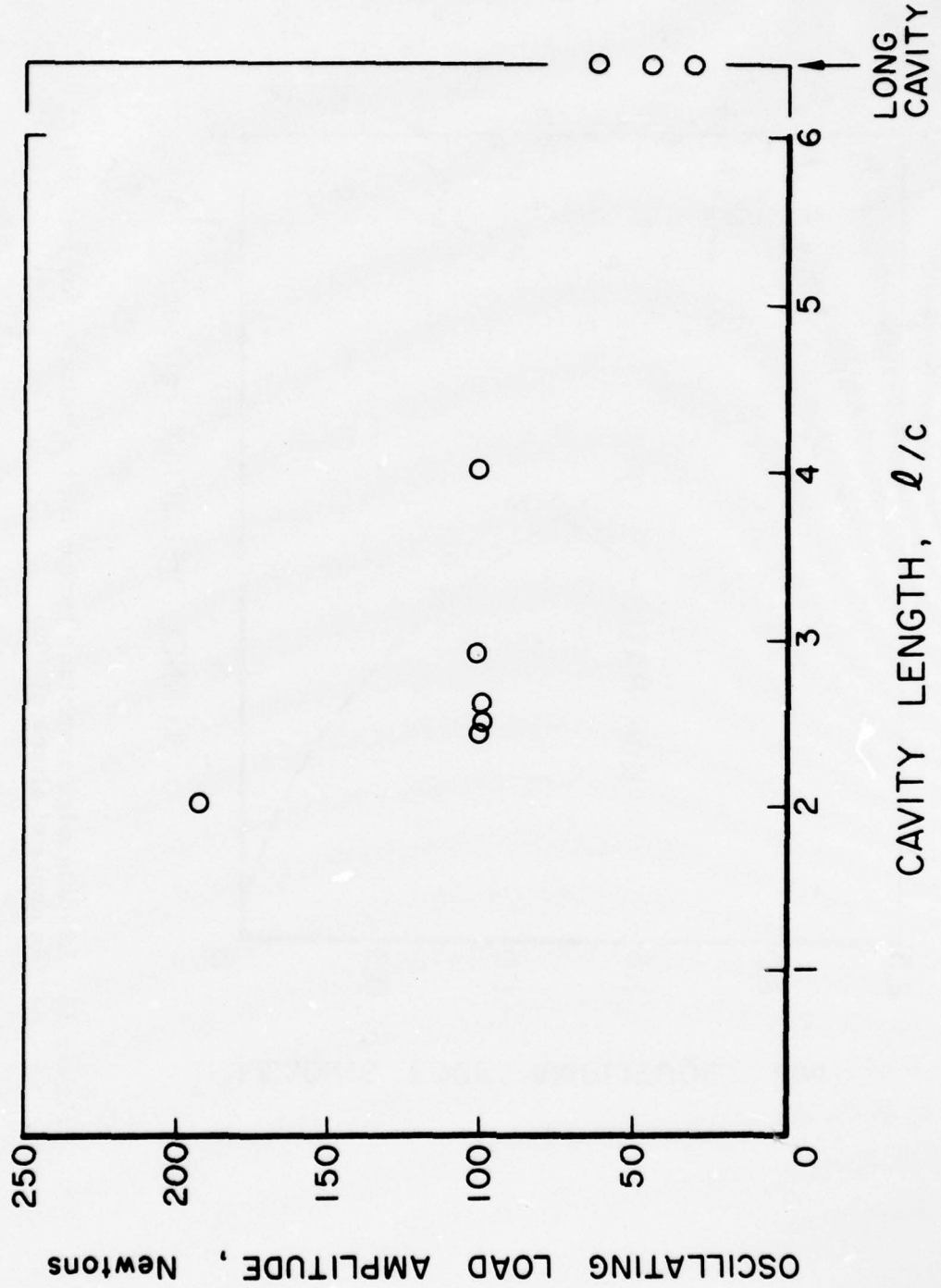

Figure 15. Oscillating load on the foil versus cavity length for foil H89 at an angle of attack of 10°.

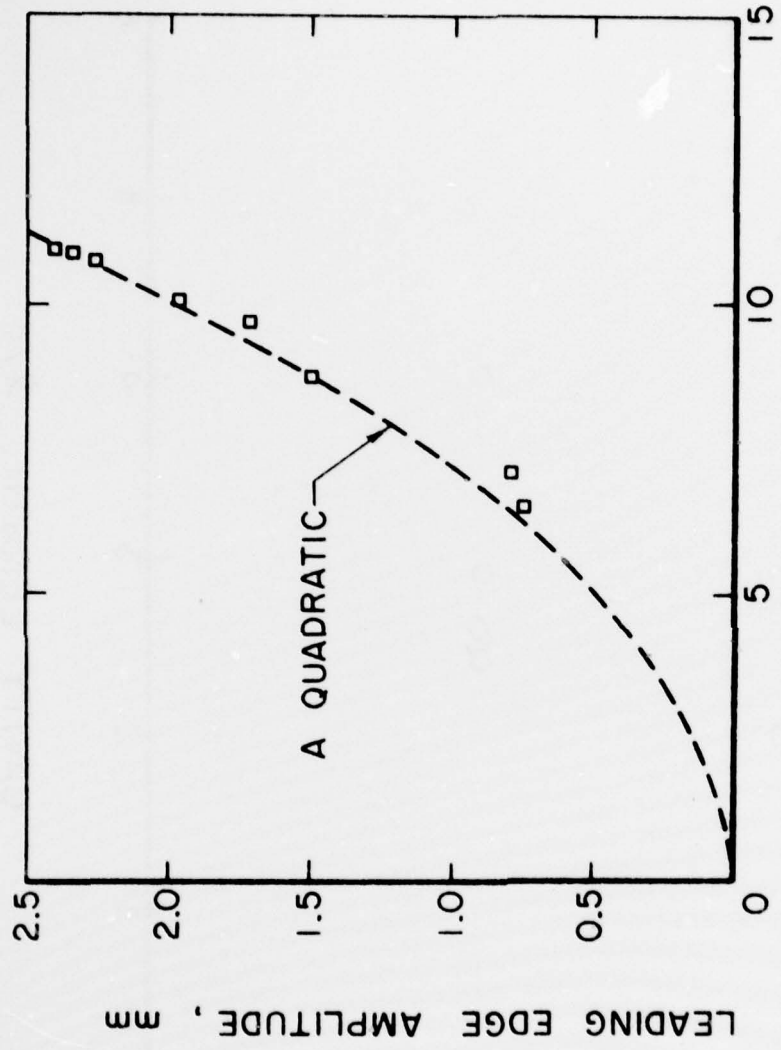

Figure 16. Leading edge amplitude versus flutter velocity for foil H89 at an angle of attack of 7°.

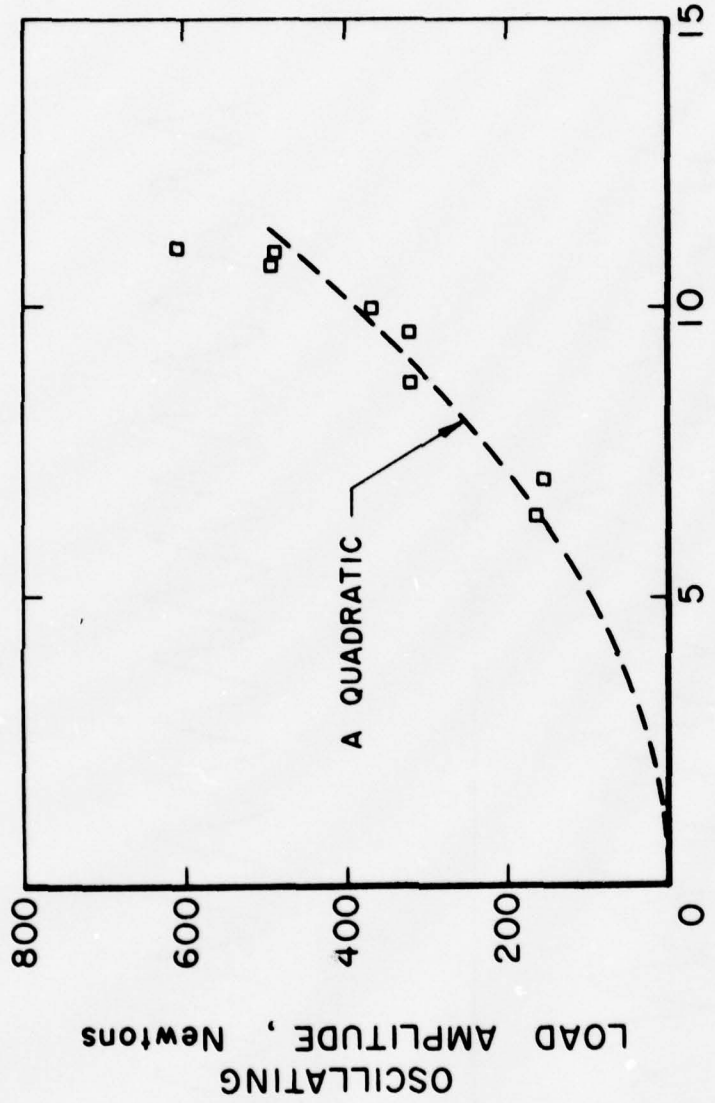

Figure 17. Oscillating load versus flutter velocity for foil H89 at an angle of attack of 7°.

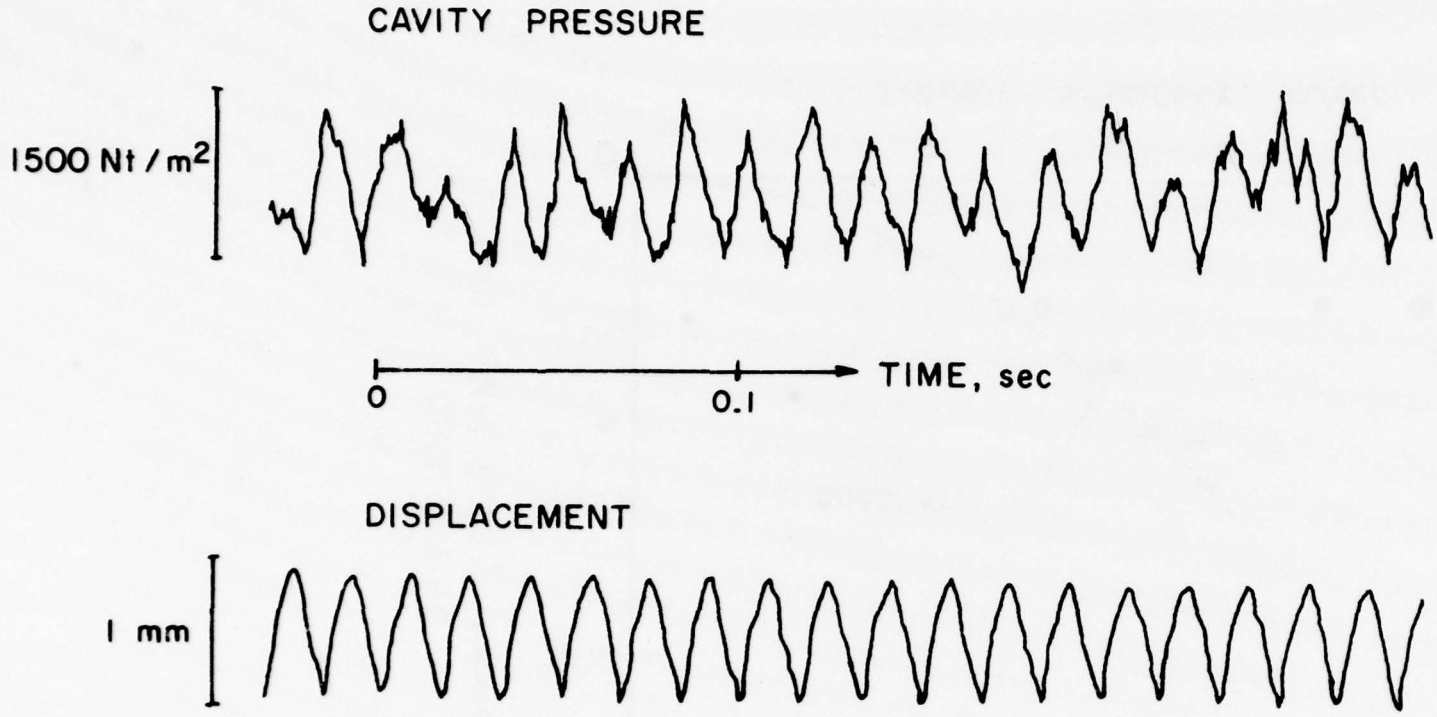

Figure 18. Typical trace of the cavity pressure as compared with the leading edge displacement during flutter (Foil H89 at $\alpha = 7^{o}$ and velocity of 9 m/sec. and $\ell/c = 2.3$)

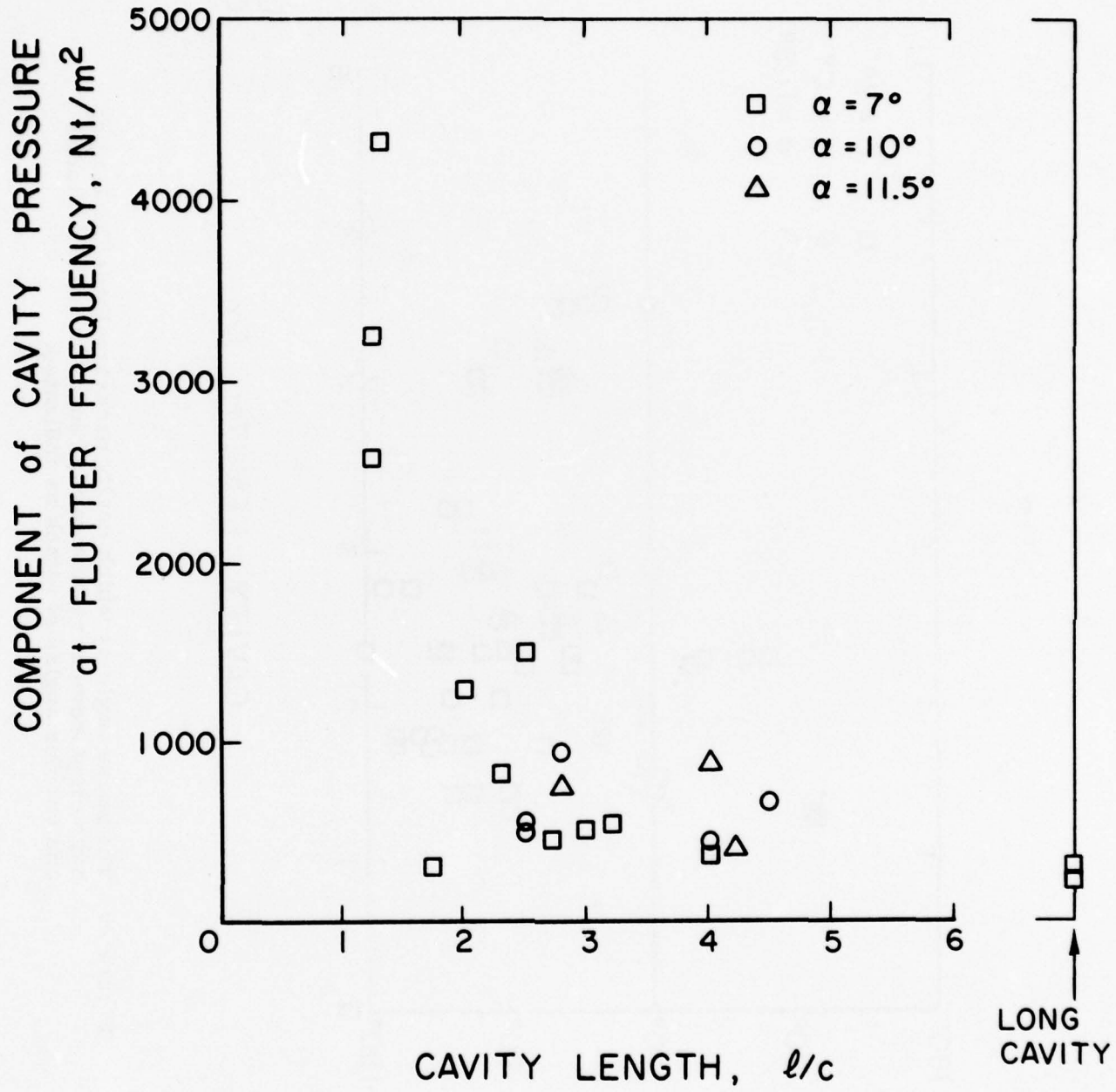

Figure 19. Magnitude of the fundamental component of the cavity pressure versus the cavity length for all HSWT foils and various angles of attack as indicated.

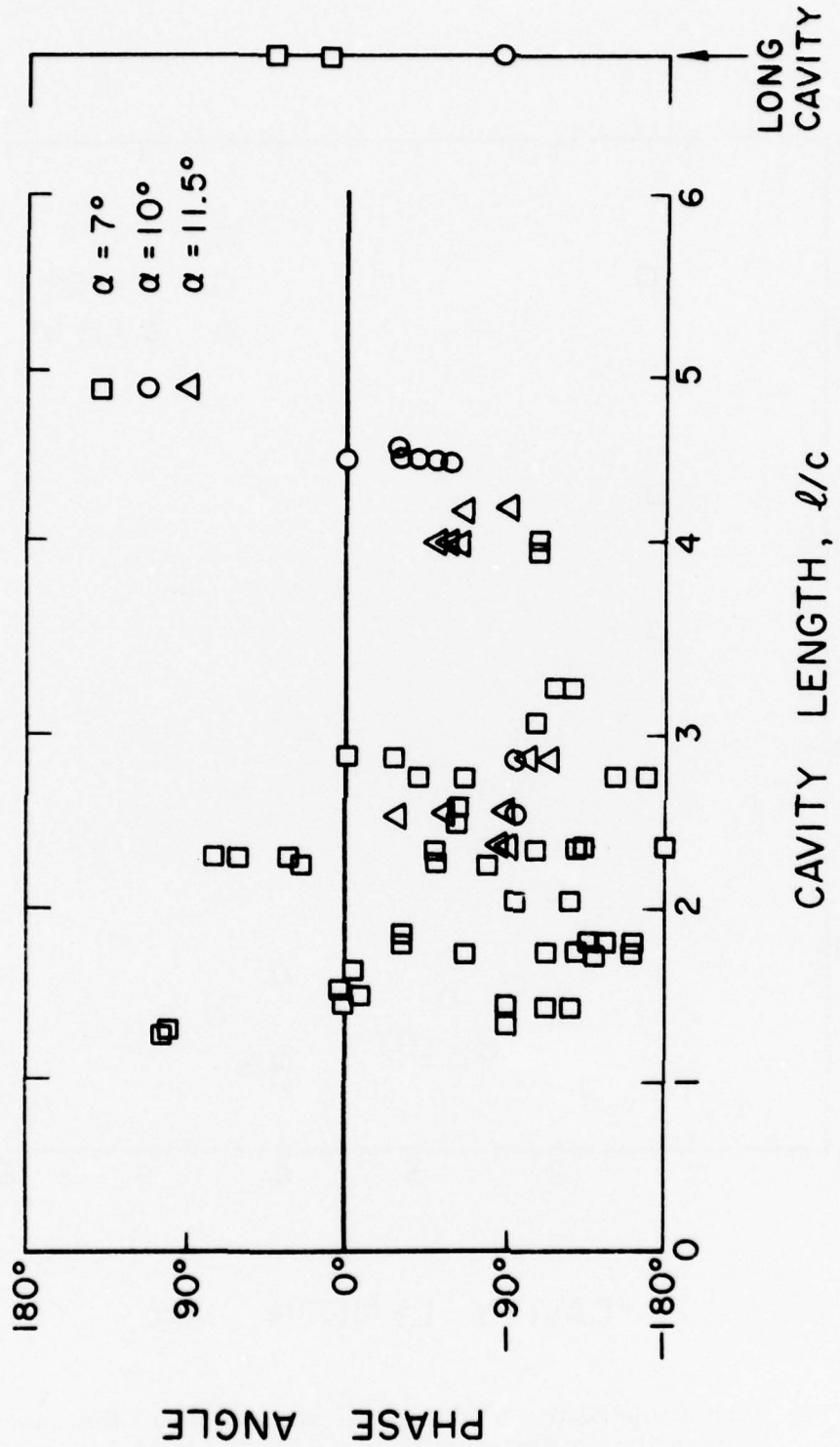

Figure 20. The phase angle by which cavity pressure leads the leading edge displacement versus cavity length for all HSWT foils and various angles of attack as indicated.

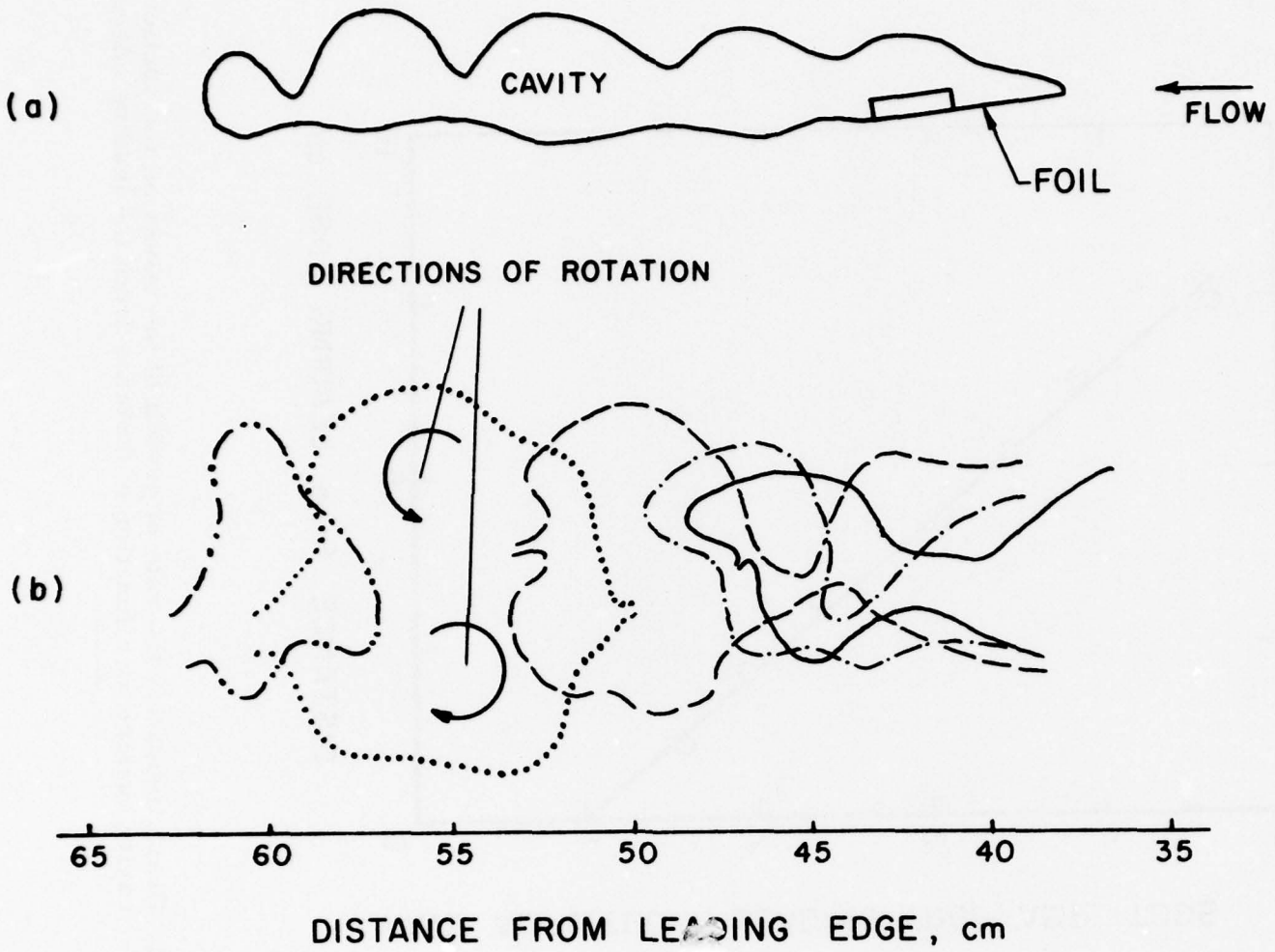

Figure 21. (a) Sketch of the form of the waves on the cavity surfaces during flutter. (b) Detailed traces of the pinch-off process in the region of cavity closure. Profiles of the end of the cavity and the pinched-off bubble are shown at times (in seconds) as follows where the origin, $t=0$, is arbitrary: $t=0$, ———; $t=0.005$, ——·——; $t=0.015$, ----; $t=0.025$, ·····; $t=0.055$, —··—. (For foil H89 at $\alpha=10^{o}$ and a velocity of 7.9 m/sec.) The pinched-off bubble seems to have opposite directions of rotation at the top and bottom as indicated by arrows.

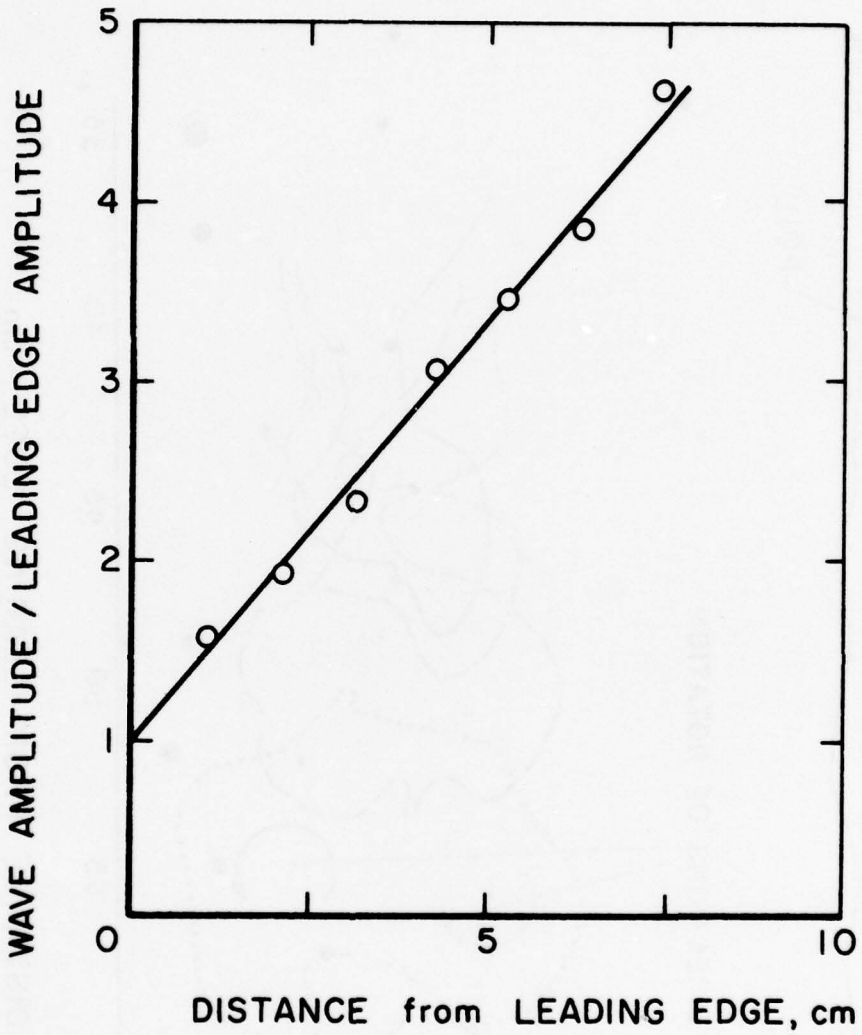

Figure 22. Graph indicating the rate of growth of the waves on the suction cavity surface as a function of distance from the leading edge.

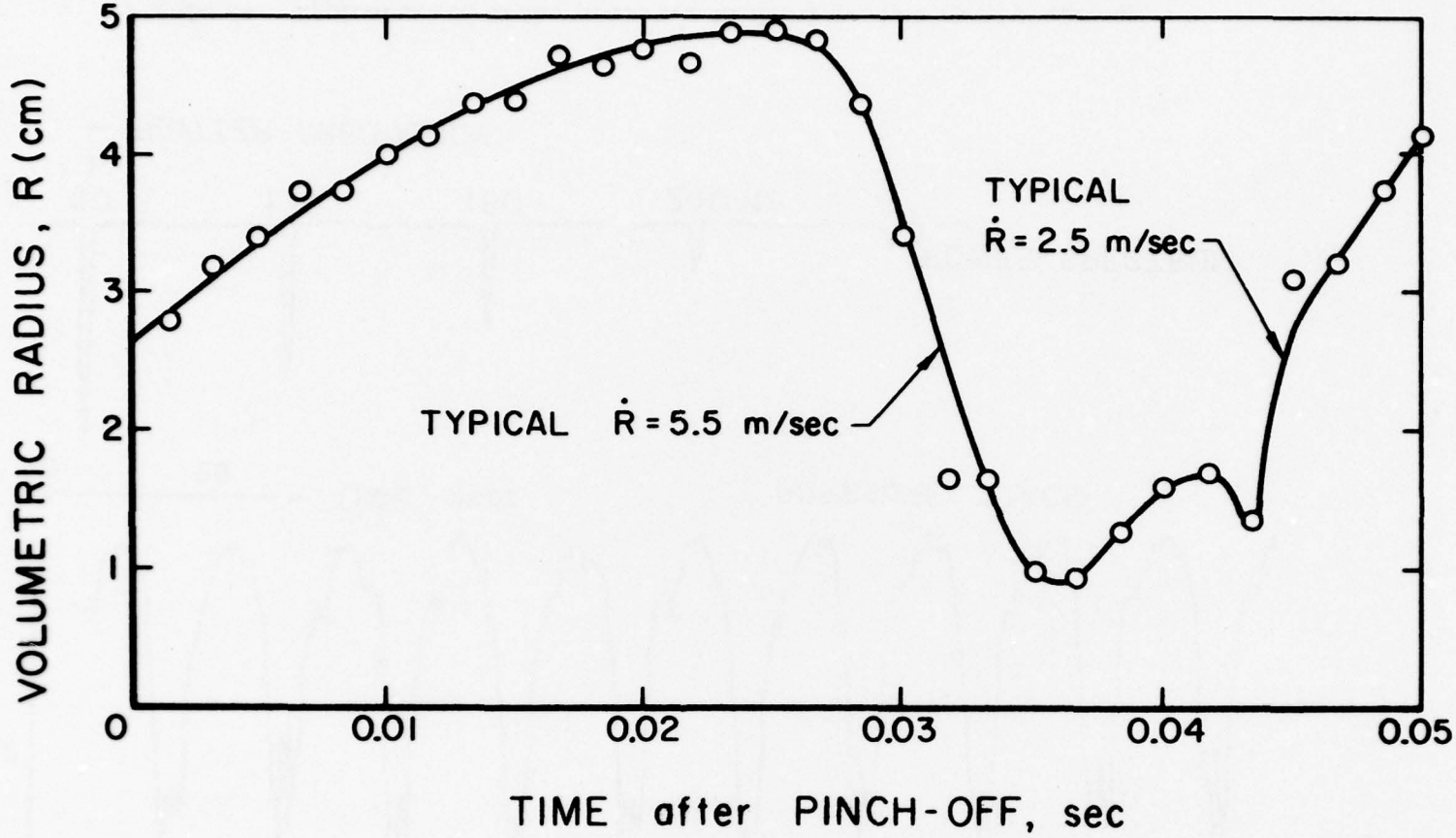

Figure 23. Volume history of the pinched-off bubble versus time from pinch off showing the first collapse and rebound. (Foil H89 , $\alpha = 10^{\circ}$, $U_F \cong 7.9$ m/sec., flutter frequency 60 Hz)

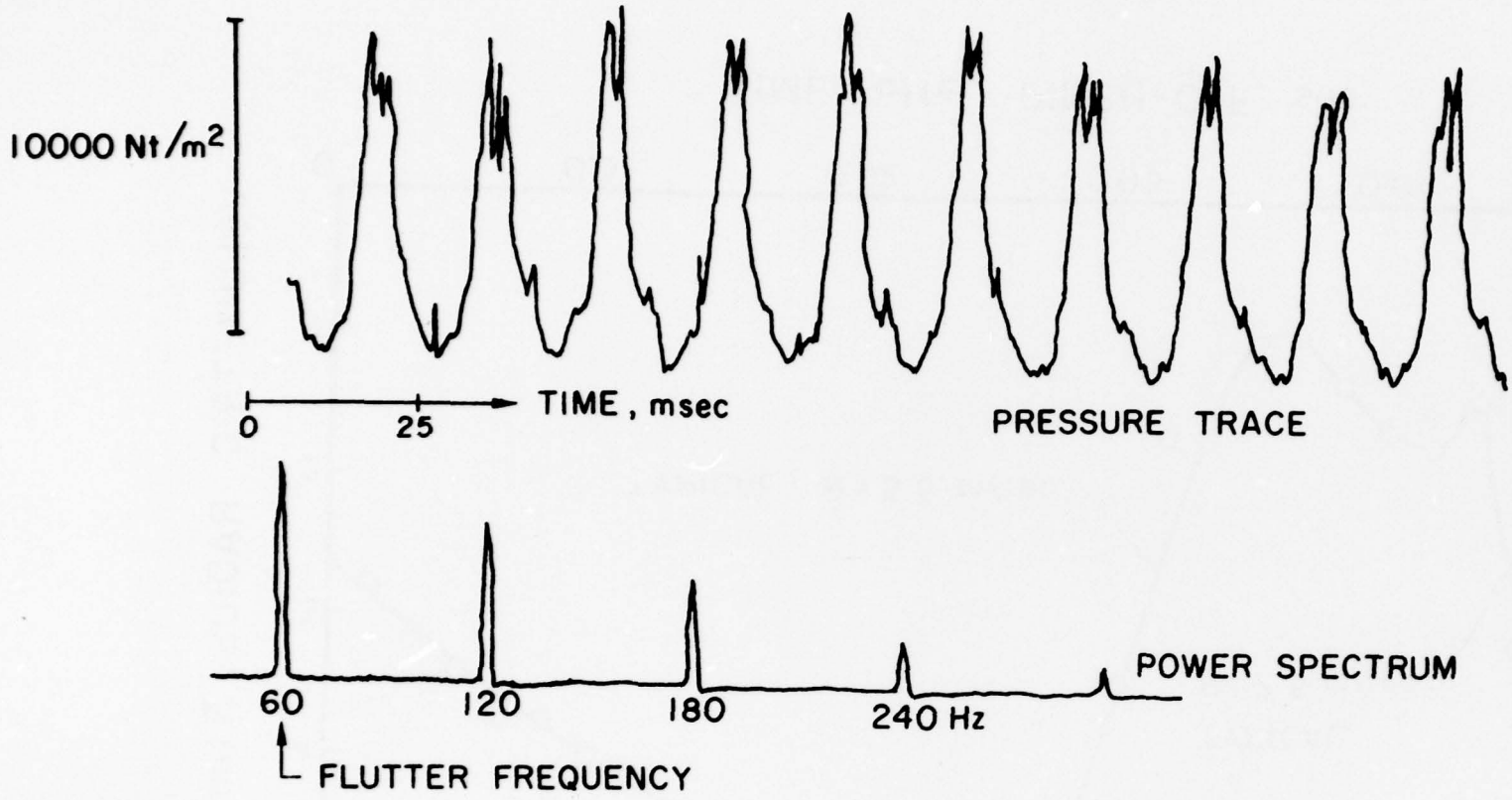

Figure 24. Typical trace of the pressure in the flow near cavity closure with its power spectrum (Foil H89, $\alpha = 7^{o}$, velocity = 8 m/sec, at a point 30 cm. downstream of cavity closure).

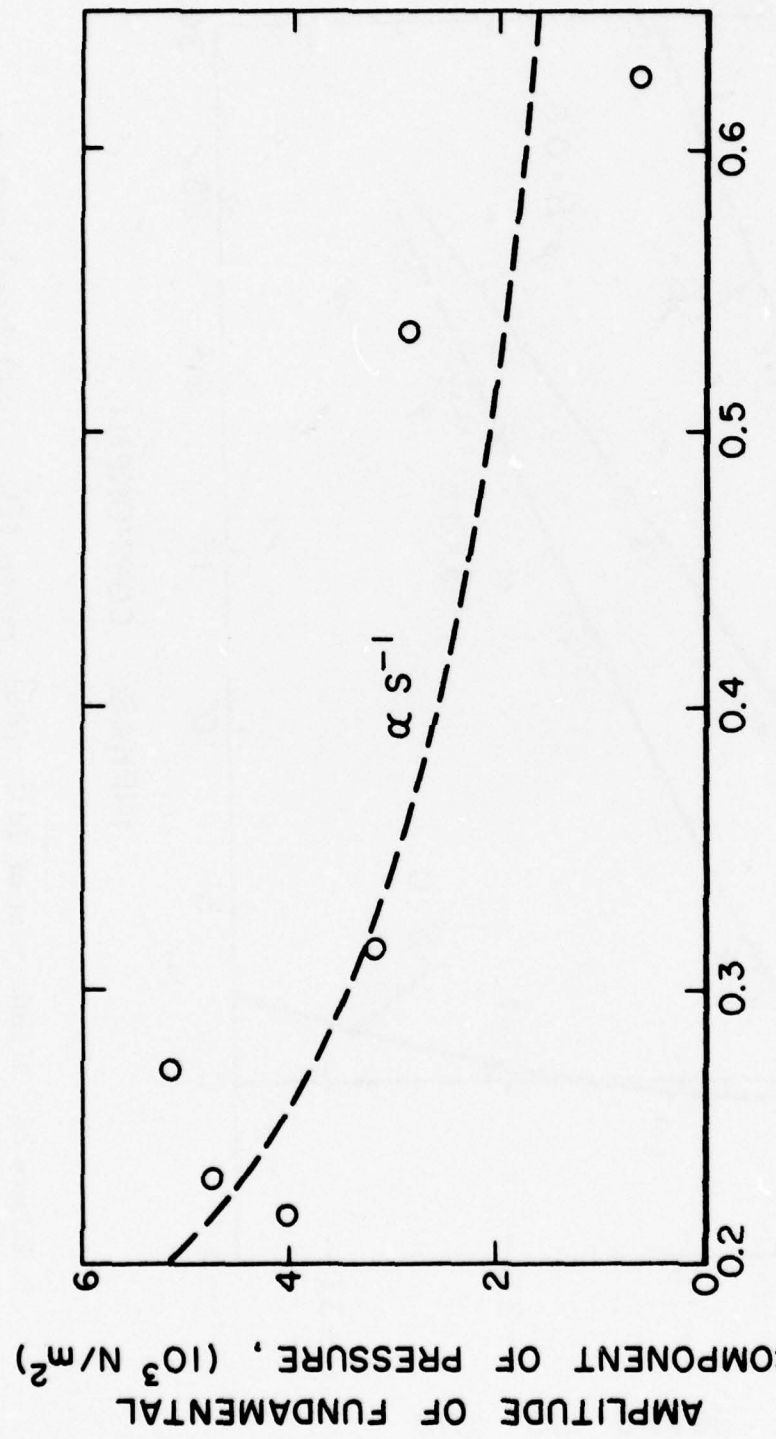

Figure 25. Magnitude of the fundamental component of pressure in the flow as a function of distance from the cavity closure region.

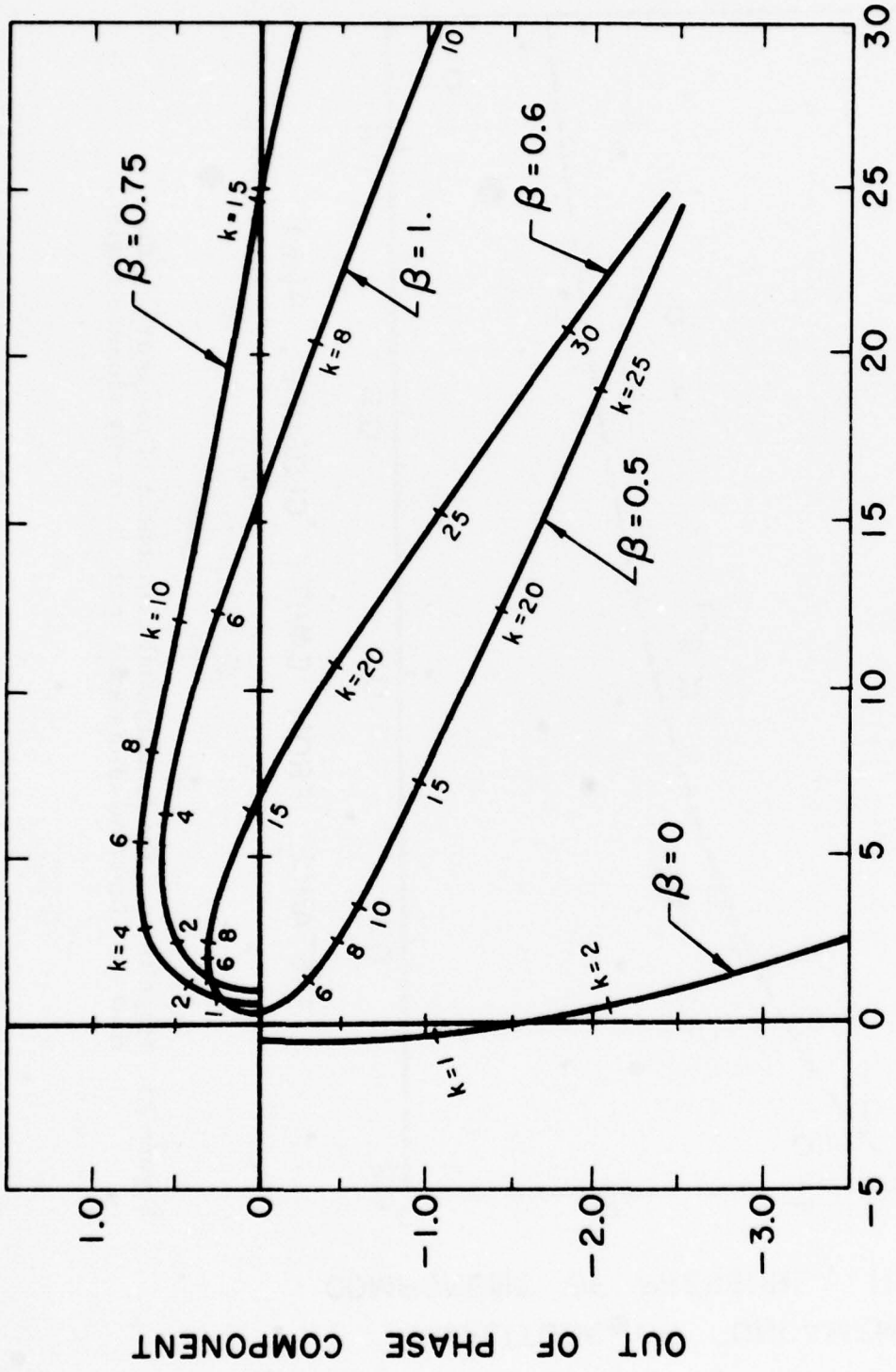

Figure 26. A polar plot of $(d\tilde{C}_{MI}/d\tilde{\alpha})$ versus $(d\tilde{C}_{MR}/d\tilde{\alpha})$ from equation (10) for various locations of the hinge; values of the reduced frequency, k, are indicated at various points along the curves.

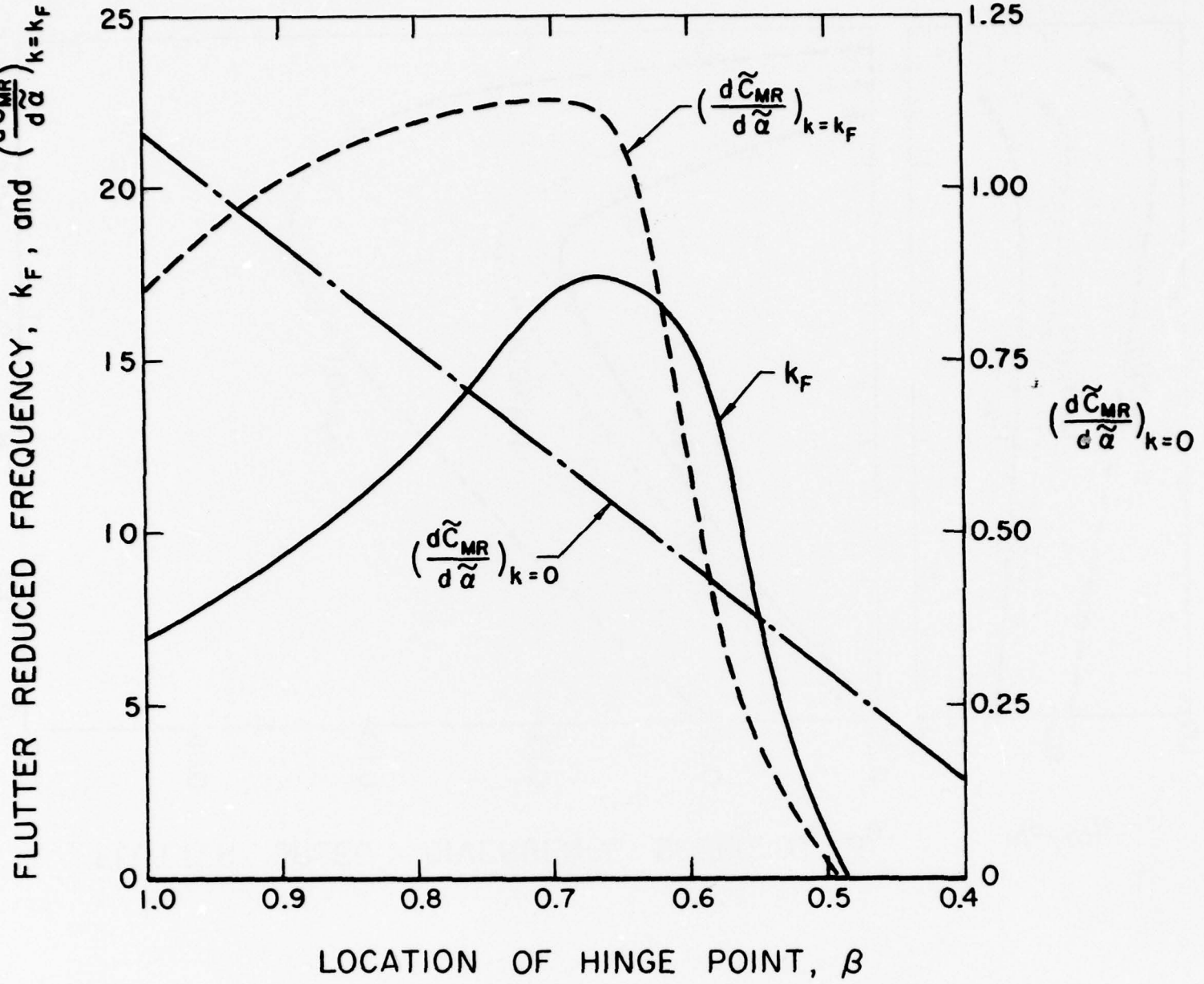

Figure 27. The reduced flutter frequency $k_F = \omega_F c/U_F$ and the values of $(d\tilde{C}_{MR}/d\tilde{\alpha})_{k=k_F}$ and $(d\tilde{C}_{MR}/d\tilde{\alpha})_{k=0}$ as functions of the hinge location.

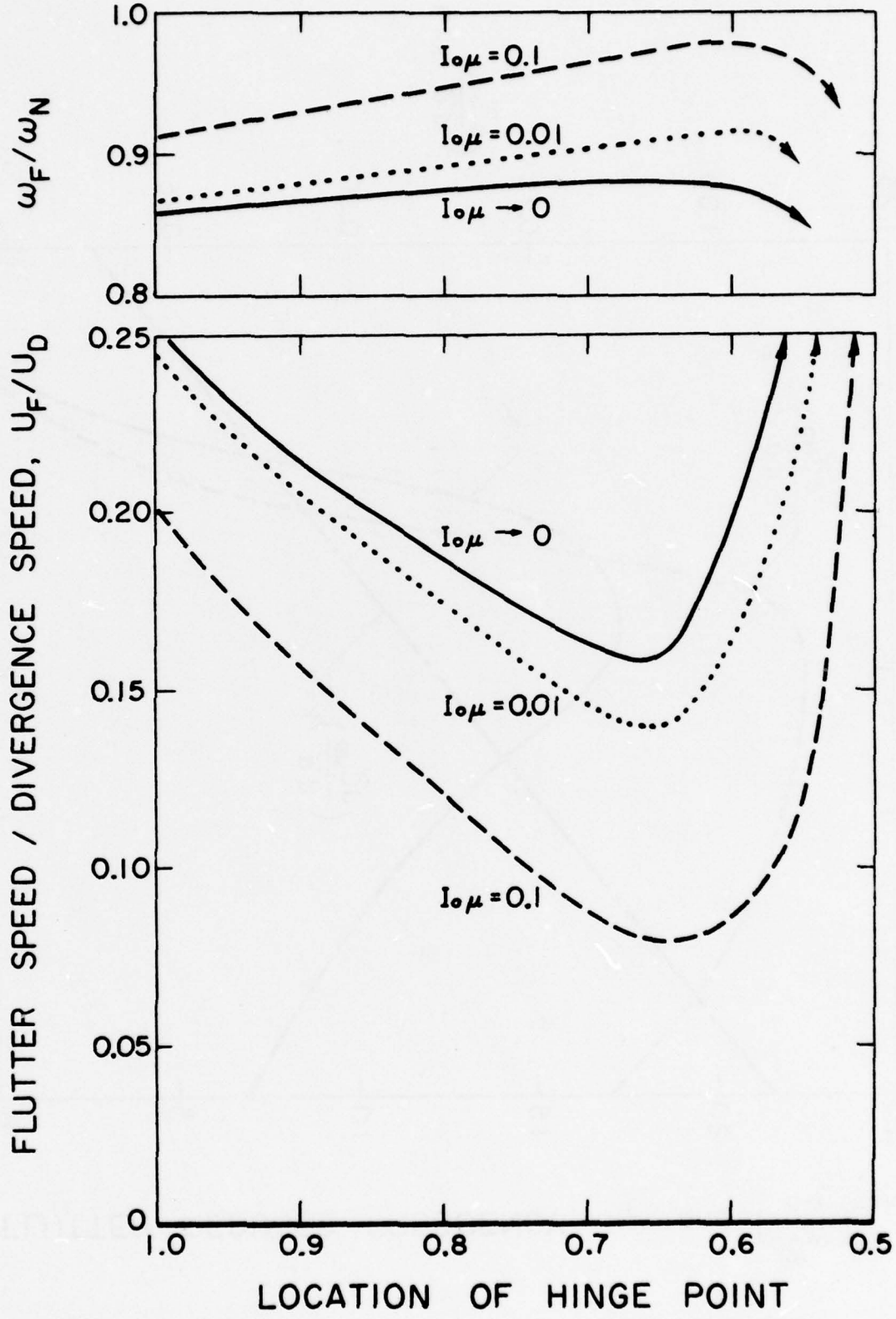

Figure 28. Values of the ratio of the flutter speed to the hypothetical divergence speed, U_F/U_D, and the ratio of the flutter frequency to the natural frequency in flows at much lower speeds, ω_F/ω_N, as functions of the hinge location for various values of $I_o\mu$.

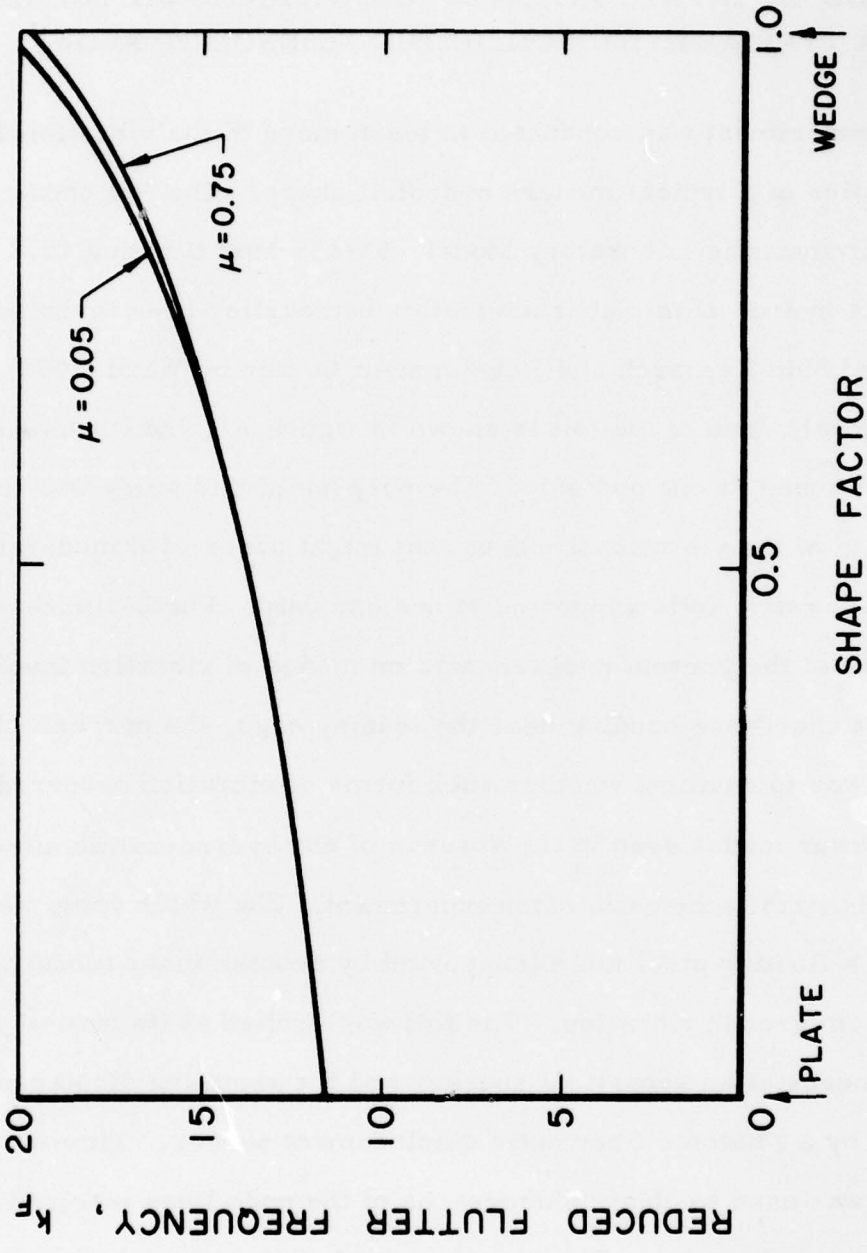

Figure 29. Reduced flutter frequency, k_F, against shape factor for foils cantilevered forward from their trailing edge according to the theory of Murai (1978) and Shimuzu (1979).

APPENDIX A

HOLOGRAPHIC INVESTIGATION OF THE VIBRATIONAL MODES OF A TYPICAL HYDROFOIL IN THE ABSENCE OF FLOW

An experiment was conducted to learn more of the vibrational characteristics of a typical modern hydrofoil shape. The foil chosen was C.I.T. Hydrodynamic Laboratory Model 35-435 Mod II with a 15.2 cm.chord and span; its hydrodynamic characteristics had earlier been investigated for the Naval Ship Research and Development Center by Ward (1976). The cross-sectional shape of the foil is shown in figure A1, and it was supported in the water tunnel at one end only. The purpose of this study was to identify some of the vibrational modes that might occur with moderate and typical aspect ratio foils supported at one end only. Furthermore since the emphasis of the present program was on modes of vibration involving predominant chordwise bending near the leading edge, the purpose of these tests was to examine whether such forms of vibration occurred as one of the lower modes even in the absence of any hydrodynamic effect. Figure A2 shows the schematic of the experiment. The whole setup was mounted on a floating steel table (supported by scooter inner tubes) to isolate it from ground vibration. The foil was excited at its natural frequency by means of an acoustical speaker and the resulting displacement was sensed by a Photonic fiber optic displacement sensor. Time-averaging holography was used to obtain photographs of the node lines involved in each of the normal modes. Figures A3 and A4 show two such photographs of vibrational modes of 860 Hz. and 1725 Hz. The supported end of the foil is at the bottom of the photographs and the leading edge is on the right hand side. The black regions on the foil represent areas of equal vibration

amplitude. Thus figure A3 shows a mode which is similar to torsional vibration. The rotational axis is somewhat behind the midchord. Figure A4 represents a higher mode which involves leading edge vibration but in which there is a significant spanwise phase change of the leading edge vibration. Figure A5 presents the modes of this foil which were observed.

The conclusion of this study was that even with foils of moderate and typical aspect ratio supported at one end, leading edge vibration occurred as one of the lower modes of oscillation.

Figure A1. Cross-section of the CIT Hydrodynamics lab hydrofoil model (35-435 mod II).

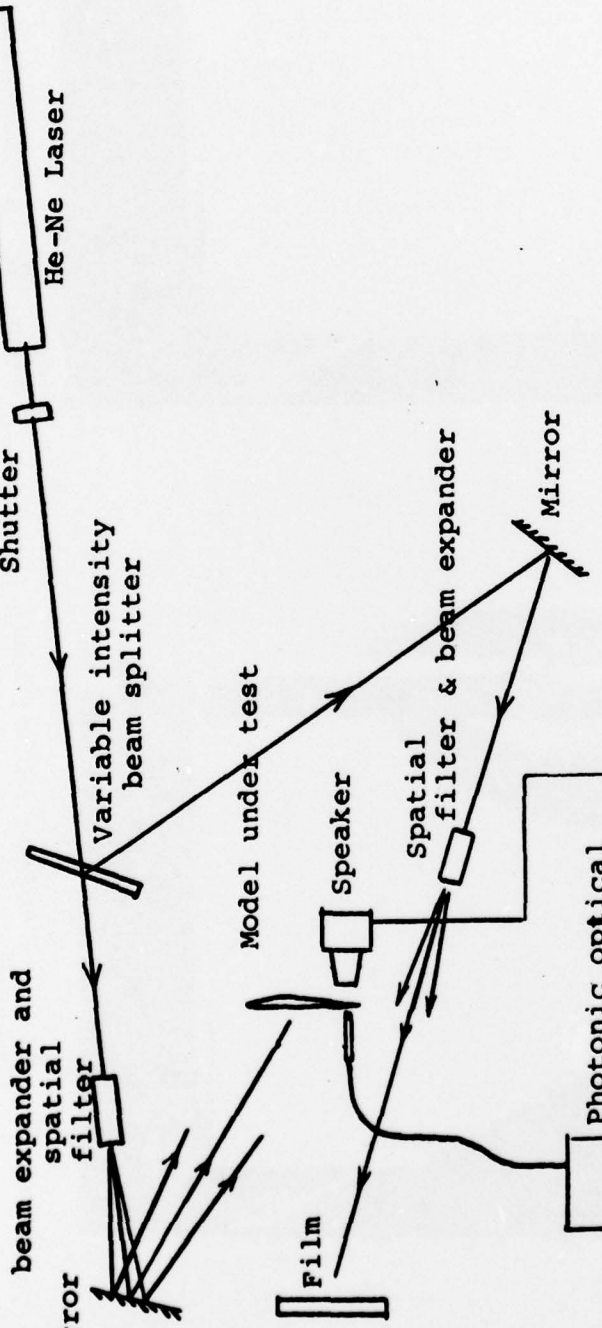

Figure A2. Schematic of the system for time-averaging holography.

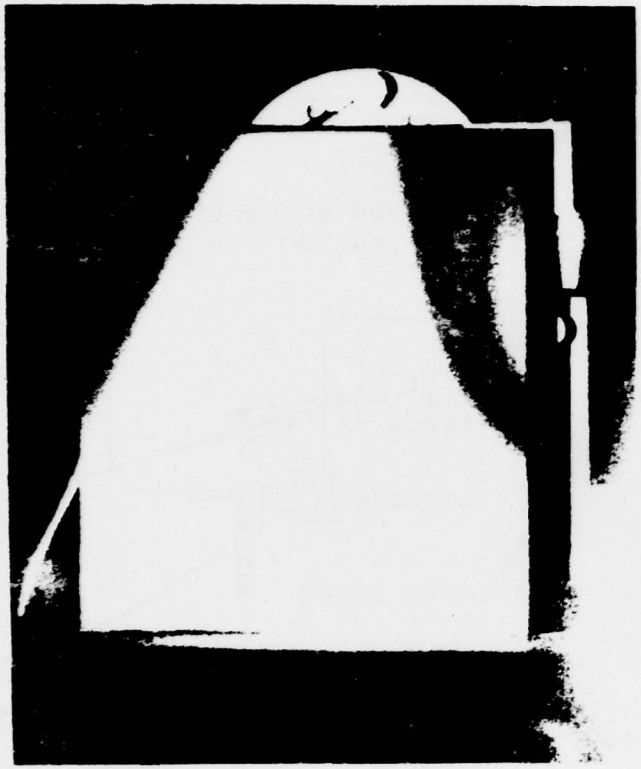

Figure A3. Vibration mode at 860 Hz; leading edge is on right, free end to the top.

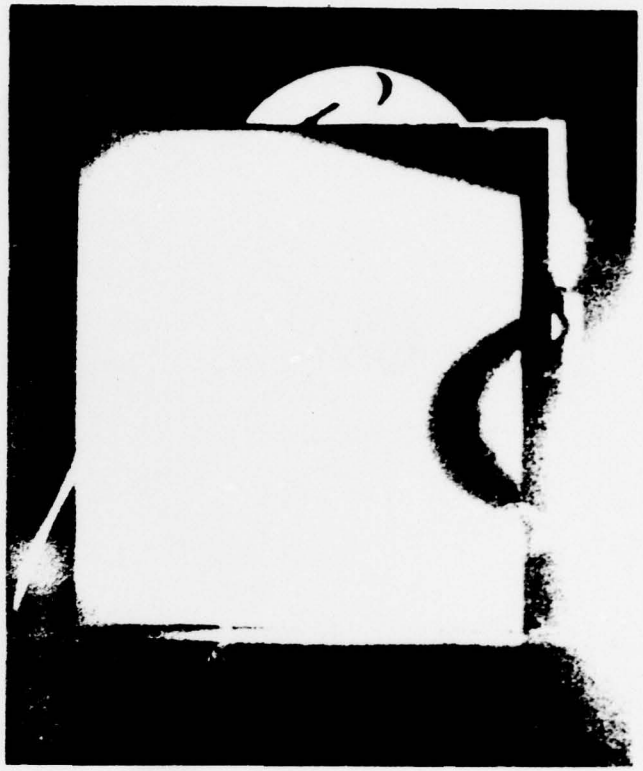

Figure A4. Vibration mode at 1725 Hz; leading edge is on right, free end to the top.

FREQUENCY	MODE	
410	SPANWISE BENDING	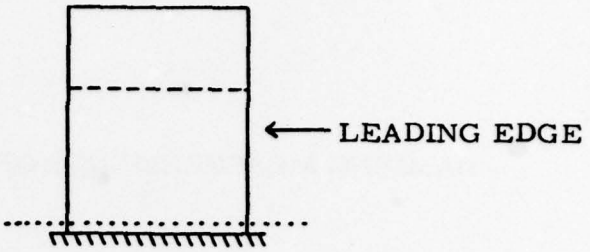
530	CHORDWISE BENDING AT LEADING EDGE TIP	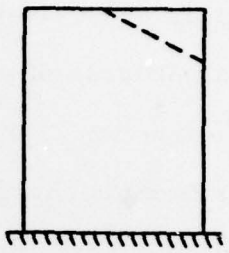
860	TORSIONAL VIBRATION	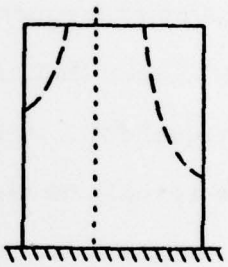
1725	CHORDWISE BENDING WITH SPANWISE PHASE CHANGE	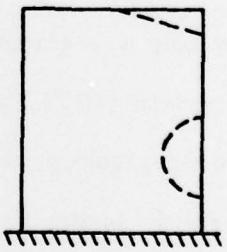
2600	CHORDWISE BENDING WITH SPANWISE PHASE CHANGE	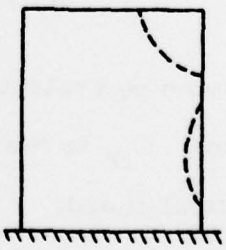

Figure A5. Natural frequencies and modes of CIT 35-435 mod II hydrofoil in air. The dashed lines are contour lines, the dotted lines are nodal lines.

APPENDIX B

DAMPING MEASUREMENTS OF THE 35.6 cm. SPAN FOILS IN STILL WATER.

During the forced vibration tests of the 35.6 cm. span foils in still water, Q-factors were obtained from the frequency response spectra for a number of amplitudes of excitation. These Q-factors are plotted in figure B1 as a function of the leading edge displacement amplitude, δ, divided by the flexible chord length, a. The resonant or natural frequencies also varied slightly with amplitude, decreasing consistently as the amplitude increased; end point frequencies for each foil are indicated in figure B1.

It can be seen that, in general, the Q-factor decreases like δ^{-1} for each individual foil. A comparison between the curves for the four different foils reveals no clear trend with stiffness or frequency. However both the δ^{-1} behavior and the frequency shift are consistent with non-linear quadratic or "velocity-squared" damping. Analysis of systems with such quadratic damping are given, for example, by Snowden (1968, p. 430) and Dinca and Teodosiu (1973, p. 278). Such damping clearly suggests a hydrodynamic drag force in the equation of motion which is proportional to $|\dot{y}|\dot{y}$ where $\dot{y}$ is the instantaneous velocity of the leading edge:

$$M\ddot{y} + C_D \tfrac{1}{2} \rho a s \, |\dot{y}| \dot{y} + Ky = F(T) \qquad \text{(B 1)}$$

Here M is some equivalent mass plus added mass, K is some equivalent spring constant, C_D is the hydrodynamic drag coefficient (rather arbitrarily based on the total chord, c, and span, s), and $F(T)$ is the applied force. It follows from the velocity-squared damping analysis that if the amplitude, δ, of the motion is small then the effective Q-factor is related to the drag coefficient by

$$\frac{1}{Q} \approx \left(\frac{32}{3\pi^2}\right)^{\frac{1}{2}} \cdot \left\{\frac{C_D \rho a s \omega_N^2}{2K}\right\} \delta \qquad \text{(B 2)}$$

where $\omega_N = (K/M)^{\frac{1}{2}}$ is the resonant frequency. Notice that as anticipated above Q is proportional to the amplitude, δ. Using equation (B 2) and the measured values of ω_N and K, drag coefficients were computed for each of the points in figure B 1 (Note: the leading edge deflection versus strain gauge output calibration is not necessary for this calculation; the values of δ and K can be put in terms of strain gauge output amplitude and static strain gauge output per unit applied load respectively). The drag coefficients are plotted in figure B 2 against the dimensionless leading edge displacement, δ/a. The large drag coefficients at very small levels of displacement are consistent with other direct measurements of the drag of plates in oscillatory flow, notably those of Keulegan and Carpenter (1958). Furthermore, like those other experimental results the drag coefficients tend to a value of the order of unity for larger displacements. This suggests a Reynolds Number effect; hence the drag coefficients have been replotted in figure B 3 against an oscillatory Reynolds number, $\omega \delta^2 / \nu$, based on tip velocity, tip displacement and the kinematic viscosity, ν, of the water. Here again the general picture seems sensible with all the large values having Reynolds numbers less than 50 and those for larger Reynolds numbers approaching unity. However the inconsistency between the foils runs through all the three figures presented; the thinner three are more consistent with each other in figure B 2 whereas the thicker three seem more consistent with each other in figure B 3.

REFERENCES

Dinca, F. and Teodosiu, C. 1973. Non-linear and random vibrations. Academic Press, Inc., N. Y. and London.

Keulegan, G. H. and Carpenter, L. H. 1958. Forces on cylinders and plates in an oscillating fluid. J. Res. Nat. Bur. Stand., Vol. 60, No. 5, pp. 423-440.

Snowden, J. C. 1968. Vibration and shock in damped mechanical systems. John Wiley and Sons, Inc., N. Y.

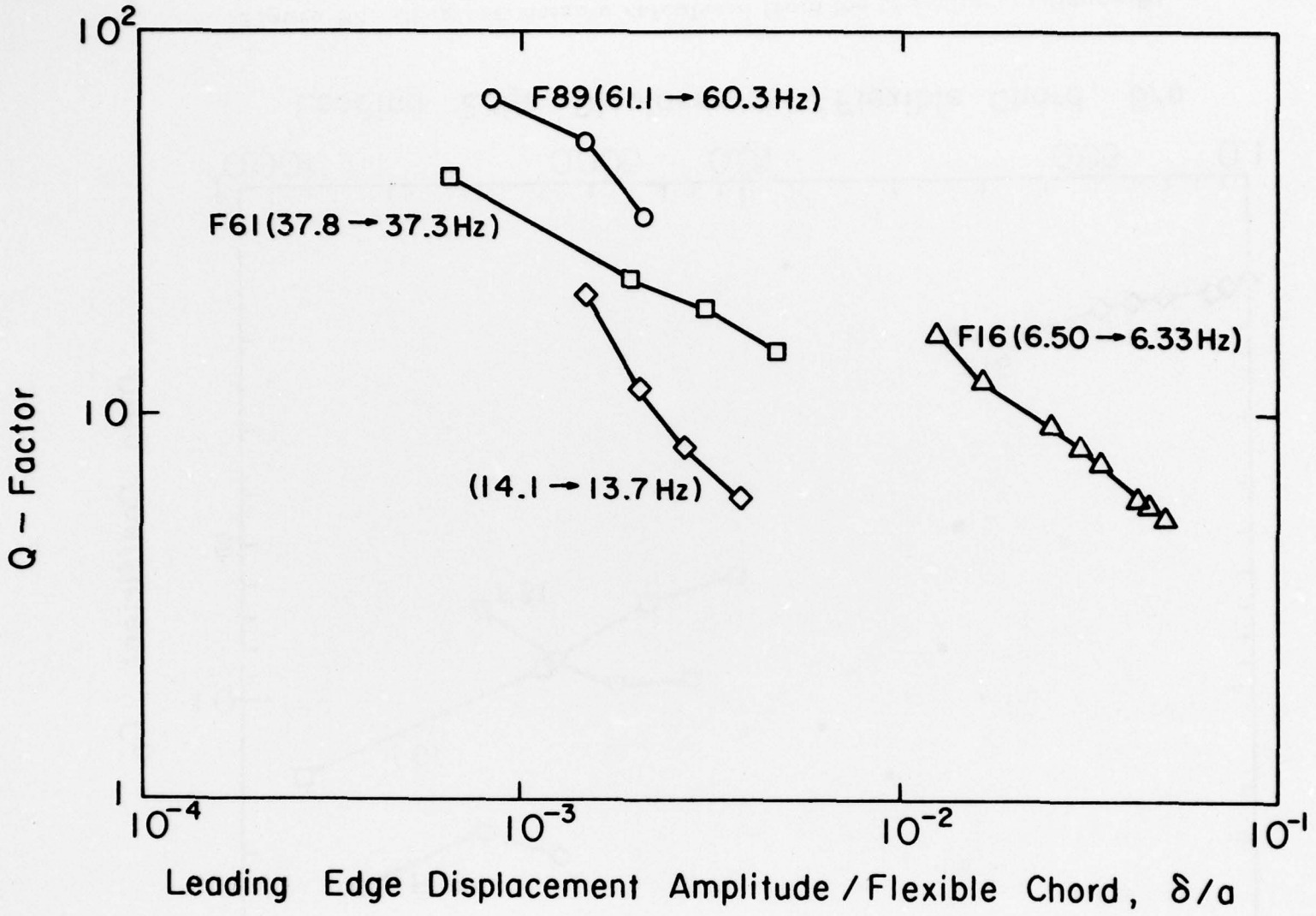

Figure B1. Q-factors for the 35.6 cm. span foils as a function of the amplitude of the leading edge displacement, δ/a. Natural frequency variations are also indicated for each foil.

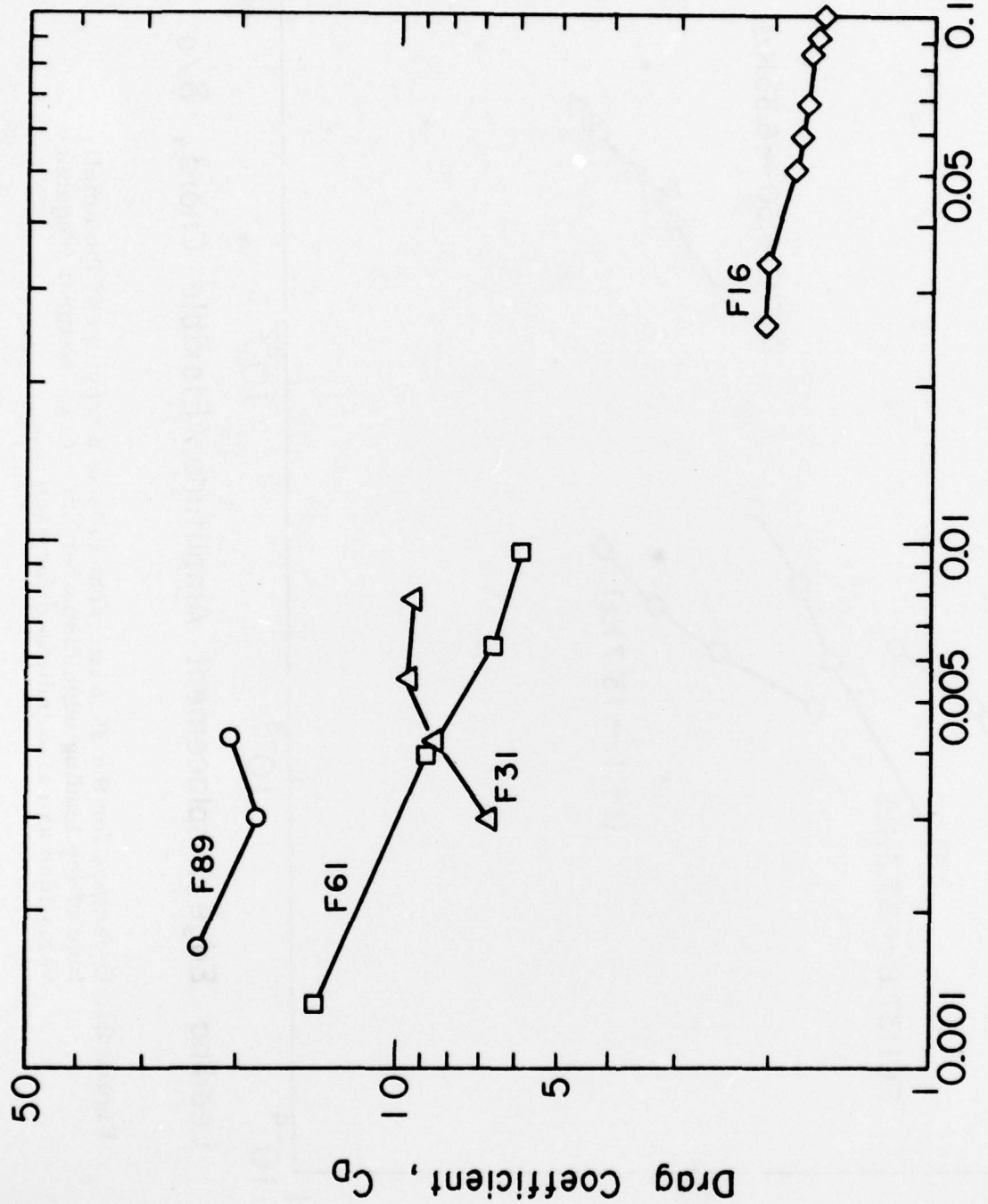

Figure B2. Drag coefficients calculated from the Q-factors of figure B1 plotted against δ/a .

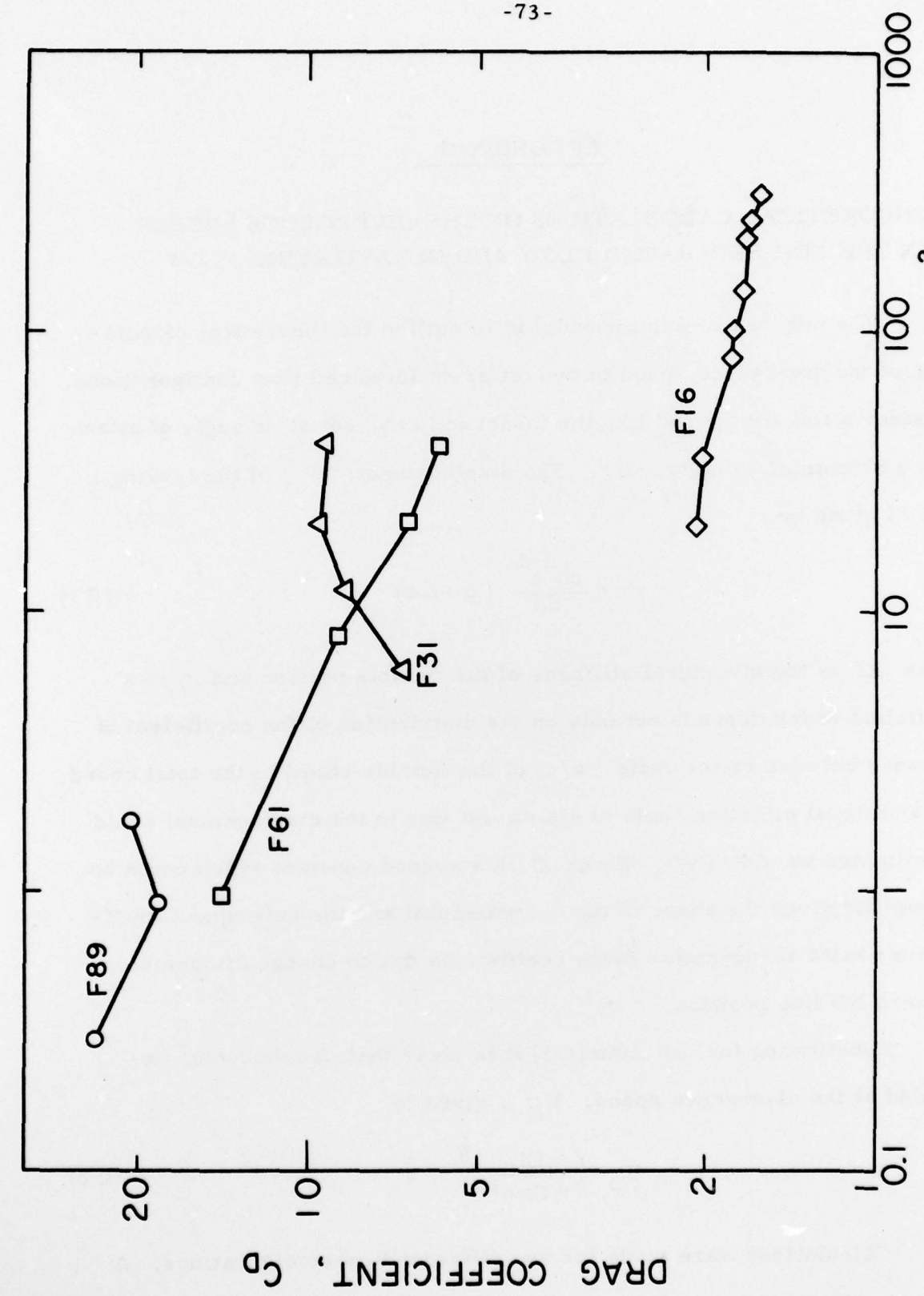

Figure B3. Drag coefficients calculated from the Q-factors of figure B1 plotted against an oscillatory Reynolds number, $\omega\delta^2/\nu$.

APPENDIX C

THEORETICAL CALCULATIONS OF THE DIVERGENCE SPEEDS IN THE NON-SEPARATED FLOW AND IN CAVITATING FLOW

The purpose of this appendix is to outline the theoretical calculations of the divergence speed in two different idealized flow configurations. Consider a foil configured like the model foils and set at an angle of attack α in a stream of velocity, U. The displacement, y, of the leading edge is given by

$$y = \eta \frac{\rho U^2 c^4}{EI} (\alpha + \Delta\alpha) \qquad (C1)$$

where EI is the structural stiffness of the flexible portion and η is a coefficient which depends not only on the distribution of the coefficient of pressure but also on the ratio a/c of the flexible chord to the total chord. The additional effective angle of attack $\Delta\alpha$ due to the displacement could be estimated as $\Delta\alpha = Cy/c$ where C is a second constant which could be determined given the shape of the deformed foil and the subsequent modifications in its aerodynamic force coefficients due to changes in camber and zero lift line position.

Substituting for $\Delta\alpha$ into (C1) it is clear that $\Delta\alpha$ becomes unbounded at the divergence speed, U_D, given by

$$U_D = \left(\frac{EI}{\eta C \rho c^3}\right)^{\frac{1}{2}} . \qquad (C2)$$

Calculations were made for two different flow configurations. A value of unity was assumed for the constant C, though in both cases the effect of camber would be to yield effective values of C somewhat less

than unity. The dashed line in figure C 1 represents the results obtained using the theoretical non-separated potential flow pressure distribution for flat plate at an angle of attack. This would not be realized in practice due to separation at the leading edge. The effect of this would be to shift the center of pressure rearwards and thus increase U_D .

By way of comparison the linearized cavity flow pressure distributions (Wu (1955, 1956)) yield the divergence speeds given by the solid lines in figure C 1; this varies somewhat with the cavitation number or cavity length and hence results are shown for lengths of 3 and 7 chords. It is expected that the cavity flow values might also be appropriate in the single phase wake flow configuration.

The numerical values for the four 35.56 cm. span foils are listed in Table 1 of the main test where the comparison with the limited observations is discussed.

REFERENCES

Wu, T. Y., 1955. A free-streamline theory for two-dimensional fully cavitated hydrofoils. CIT Hydrodynamics Lab. Rep. No. 21-17, July 1955.

Wu, T. Y., 1956. A note on the linear and non-linear theories for fully cavitated hydrofoils. CIT Hydrodynamics Lab. Rep. No. 21-22, August 1956.

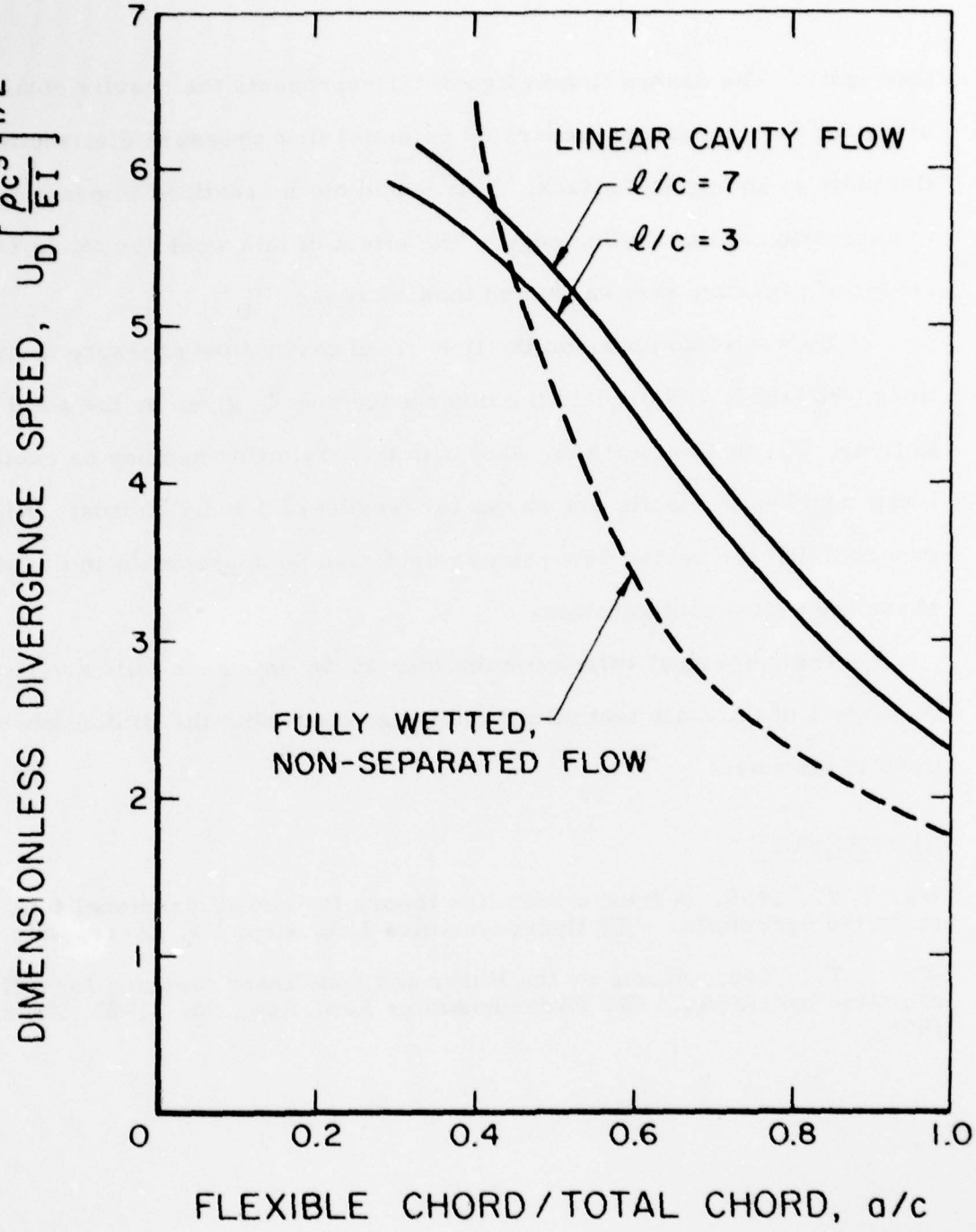

Figure C1. The theoretical and dimensionless divergence speed, $U_D[\rho c^3/EI]^{\frac{1}{2}}$, as a function of the flexible chord to total chord ratio, a/c , for fully wetted, non-separated flow and for linear cavity flow (for cavity length/chord ratio of 3 and 7)

APPENDIX D

SOME WAKE PRESSURE SPECTRAL INFORMATION

During the HSWT tests without cavitation some information was obtained on the pressure in the wake behind foil H68 using a piezo-electric pressure transducer attached to the mounting bar. A typical trace at a tunnel velocity of 5.5 m/sec. and an angle of attack of 7^{o} is included in figure D1; the output from the foil strain gauges under these conditions was negligible. Spectral analysis of the wake pressure (see figure D) revealed a noisy signal with a peak at the natural foil frequency of 36 Hz (under cavitating conditions the natural foil frequency was somewhat higher at about 44 Hz). The qualitative features of this pressure were quite unlike those of water pressure or foil strain gauge signals at or near flutter in a cavitating flow. The latter were invariably quite sinusoidal with a very dominant peak in the spectra at the natural frequency.

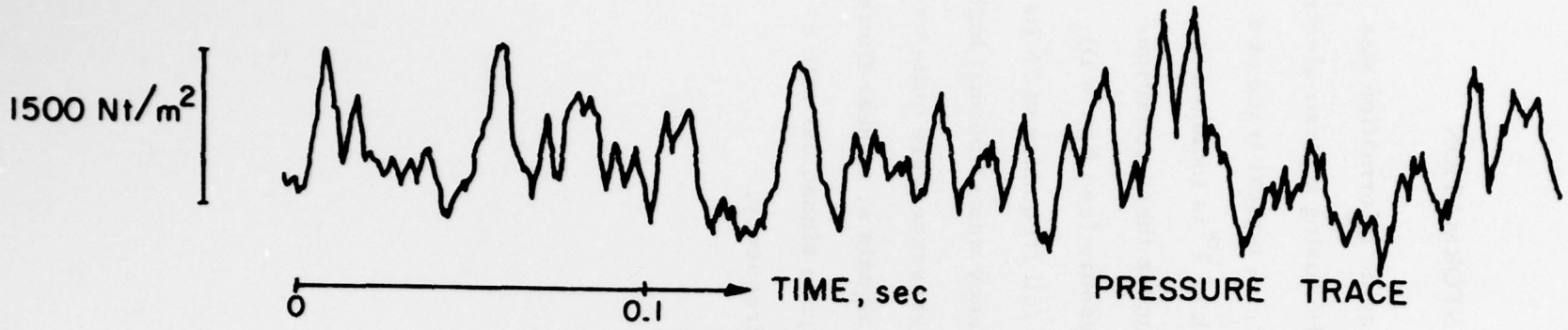

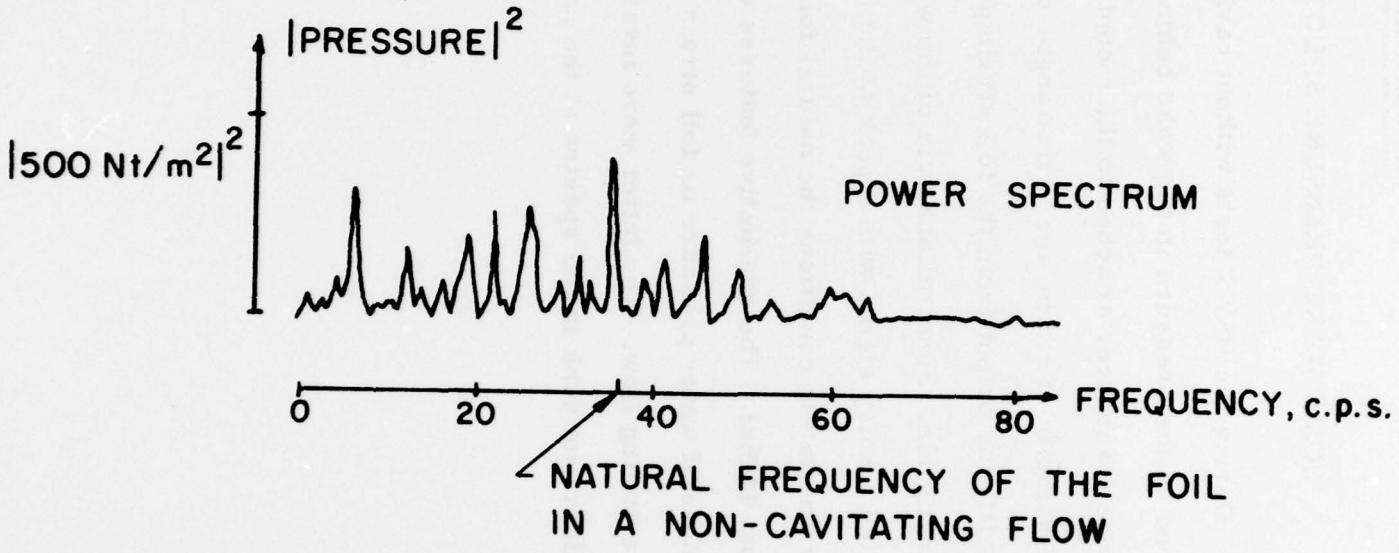

Figure D1. Typical wake flow pressure trace (above) for foil H68 at 18 ft./sec. and $\alpha = 7^{o}$. The spectrum is shown below where the natural frequency (36 Hz) is indicated. (Foil H68 at 4.6 m/sec., $\alpha = 7^{o}$)